

A Radiative Transfer Framework for Spatially-Correlated Materials

ADRIAN JARABO, Universidad de Zaragoza – I3A

CARLOS ALIAGA, Universidad de Zaragoza – I3A, and Desilico Labs

DIEGO GUTIERREZ, Universidad de Zaragoza – I3A



Fig. 1. Spatial correlation in media leads to non-exponential light transport, which significantly affects appearance. The image shows volumetric renderings of translucent dragons made of materials with the same density per unit differential volume $\bar{\mu} = 10$ (isotropic, albedo $\Lambda = .8$), but different correlations. Left: using classic light transport, where material particles are assumed to be uncorrelated. Middle and right: positive and negative correlation, respectively, using our novel framework for spatially-correlated materials. The insets show illustrative views of scatterer correlation for each dragon.

We introduce a non-exponential radiative framework that takes into account the local spatial correlation of scattering particles in a medium. Most previous works in graphics have ignored this, assuming uncorrelated media with a uniform, random local distribution of particles. However, positive and negative correlation lead to slower- and faster-than-exponential attenuation respectively, which cannot be predicted by the Beer-Lambert law. As our results show, this has a major effect on extinction, and thus appearance. From recent advances in neutron transport, we first introduce our Extended Generalized Boltzmann Equation, and develop a general framework for light transport in correlated media. We lift the limitations of the original formulation, including an analysis of the boundary conditions, and present a model suitable for computer graphics, based on optical properties of the media and statistical distributions of scatterers. In addition, we present an analytic expression for transmittance in the case of positive correlation, and show how to incorporate it efficiently into a Monte Carlo renderer. We show results with a wide range of both positive and negative correlation, and demonstrate the differences compared to classic light transport.

CCS Concepts: • **Computing methodologies** → **Rendering**; *Reflectance modeling*;

Additional Key Words and Phrases: Spatially-Correlated Transport, Non-Exponential Light Transport, Correlated Radiative Transfer

ACM Reference format:

Adrian Jarabo, Carlos Aliaga, and Diego Gutierrez. 2018. A Radiative Transfer Framework for Spatially-Correlated Materials. *ACM Trans. Graph.* 37, 4, Article 78 (August 2018), 13 pages. <https://doi.org/10.1145/3197517.3201282>

© 2018 Association for Computing Machinery. This is the author's version of the work. It is posted here for your personal use. Not for redistribution. The definitive Version of Record was published in *ACM Transactions on Graphics*, <https://doi.org/10.1145/3197517.3201282>.

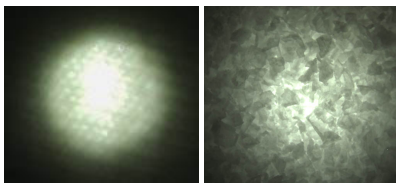
1 INTRODUCTION

Volumetric appearances are ubiquitous in the real world, from translucent organic materials to clouds, smoke, or densely packed granular media. Voxel-based representations with anisotropic scattering functions [Heitz et al. 2015; Jakob et al. 2010] have been widely used in recent years to represent the appearance of complex geometries such as trees [Loubet and Neyret 2017; Neyret 1998], cloth and hair [Aliaga et al. 2017; Khungurn et al. 2015; Schröder et al. 2011; Zhao et al. 2011], or particles' aggregates [Meng et al. 2015; Moon et al. 2007; Müller et al. 2016].

Many translucent objects and participating media present a strong spatial correlation between scatterers¹ [Coquard and Baillis 2006; Knyazikhin et al. 1998; Lovejoy et al. 1995], where scatterers' densities are non-uniform within a differential volume. The aerosol of clouds, for instance, tends to form clusters, resulting in areas with very different optical thicknesses [Marshak et al. 1998]. As a result, the probability of a photon interacting with a scatterer inside each differential volume is also non-uniform, which in turn has a great effect in the final appearance, as Figure 1 shows.

Most previous works in graphics have assumed an uncorrelated distribution of scatterers, considering only spatial correlation at a macroscopic scale as heterogeneous media. This results in the well-known exponential transmittance predicted by the Beer-Lambert law. However, in the presence of correlation at differential-volume scale, the predictions of the Radiative Transfer Equation (RTE) [Chandrasekhar 1960] break, and therefore attenuation is no longer exponential (see Figure 2): In such cases, negatively correlated media

¹Following other works' terminology, through the paper we use the term "scatterers" for all particles in the media, including perfect absorbers.



| Media | R^2 |
|--------------|-------|
| Milk* | 0.99 |
| Black Fabric | 0.87 |
| White Fabric | 0.76 |
| Maldon Salt | 0.76 |
| Sugar | 0.69 |

Fig. 2. Left: Photographs of spatially-correlated media (white fabric, and Maldon salt), lit from behind using a mobile flash. Right: We evaluate the transmittance of different media, by fitting measurements at different optical thickness to the exponential decay predicted by the classic Beer-Lambert law. As expected, a diluted liquid such as milk (marked with an asterisk) shows a very close fit to the exponential decay (measured using the R^2 metric); however, transmittance in locally correlated media cannot be modeled using classic radiative transfer. Details on the experiment can be found in Section S.11.

leads to *faster-than-exponential* transmittance, whereas positive correlation leads to *slower-than-exponential* transmittance [Davis et al. 1999]. Works rendering granular aggregates observed such non-exponential transmittance; however, they either formulate it in an uncorrelated radiative (exponential) framework [Meng et al. 2015], precalculate the full light transport explicitly [Moon et al. 2007], or combine both approaches [Müller et al. 2016].

In this work we introduce a theoretical framework for simulating light transport in spatially-correlated media, which accounts for the local structure of scatterers. Our framework builds upon the well-established radiative theory, and leverages recent advances in *non-classical transport* in the neutron transport field: We extend the Generalized Boltzmann Equation (GBE) [Larsen 2007], which generalizes the RTE to correlated media, and lift its main limitations, leading to a general framework suitable for computer graphics. In addition, we present an analytic expression of transmittance for positive correlation, leading to a compact representation of directionally-dependent spatial correlation based on a gamma distribution of scatterers. We also present efficient sampling techniques, enabling the use of our model within any existing volumetric renderer. Our framework is able to accurately simulate light transport inside correlated media. We show results with a wide range of correlations, both negative and positive, and demonstrate the differences with classic (uncorrelated) light transport. Our model is general and intuitive, and can be seen as complementary in the spatial domain to angular anisotropy in media [Heitz et al. 2015; Jakob et al. 2010]. It might also be useful in other areas such as volumetric level of detail, or accelerating light transport using similarity theory.

Overview The technical sections of the paper are organized as follows: We first present a general background of radiative transport in uncorrelated media, a brief summary of the effect of spatial correlation on extinction, and the Generalized Boltzmann Equation (Section 3). Unfortunately, the original formulation of the GBE presents some simplifying assumptions valid for neutron transport in reactors, but which limit its applicability in rendering. In Section 4 we present our Extended GBE, which lifts the limitations of the original GBE to support more general media, and include a thorough analysis of its boundary conditions. Finally, in Section 5

we propose an appearance model for positively correlated media based on local optical parameters, which is intuitive and easy to manipulate, and which can be plugged directly into our Extended GBE.

2 RELATED WORK

Volumetric light transport Simulating light transport in participating media has a long history in computer graphics (see e.g. [Gutierrez et al. 2008]). Existing methods aim to efficiently solve the RTE [Chandrasekhar 1960] by means of path tracing [Lafortune and Willems 1996; Veach 1997], photon mapping [Jensen 2001], photon beams [Jarosz et al. 2011], or a combination of these techniques [Křivánek et al. 2014]. Our framework is independent of the particular algorithm used for rendering. Jakob et al. [2010] extended the RTE to account for directional (angular) anisotropy. Later, Heitz et al. [2015] further extended this model with the SGGX microflakes distribution. While these works focus on the local angular dependence of scattering and extinction, they still assume that the scatterers are uncorrelated, distributed uniformly in the spatial domain. Our work is orthogonal to these approaches, focusing on the effects of spatial correlation.

Volumetric representation of appearance Volumetric representations of explicit geometry have been successfully used to approximate complex appearances. Meng et al. [2015] used a classical radiative approximation of light transport in particulate media for efficient rendering. Fiber-level cloth appearance models based either on micro-CT geometry [Zhao et al. 2011, 2012] or procedural modeling [Schröder et al. 2011], have used volumetric anisotropic representations for rendering high-detailed garments [Aliaga et al. 2017], similar in quality to explicit fiber representations [Khungurn et al. 2015]. Zhao et al. [2016] presented an optimization-based approach to downsample volumetric appearance representation by altering the rendering parameters (scattering and phase function) to match the desired appearance. All these works make again the assumption of perfect decorrelation of the scatterers in the medium. Our theoretical framework departs from this assumption.

Correlated volumetric media Correlated volumetric media have been studied in computational transport in fields such as nuclear engineering [Camminady et al. 2017; Larsen and Vasques 2011; Levermore et al. 1986], atmospheric sciences [Davis and Marshak 2004; Davis et al. 1999; Newman et al. 1995], or thermal propagation [Bellet et al. 2009; Coquard and Baillis 2006; Taine et al. 2010], leading to *non-classical* transport theories [Frank and Goudon 2010; Larsen 2007]. Non-classical transport has been however largely unexplored in graphics: The first work modeling non-exponential flights in graphics is the work of Moon et al. [2007], which pre-computed transport functions of granular materials as a set of homogeneous shells. However, they required precomputing all light transport operators rather than attempting to express such non-exponential flights into a new radiative transport theory, and did not take into account the effect of correlation at boundaries. Müller et al. [2016] later used a similar approach in combination with other volumetric estimators for rendering heterogeneous discrete media. Concurrently to us, Wrenninge et al. [2017] used non-exponential flights for increased artist control on volumetric light transport,

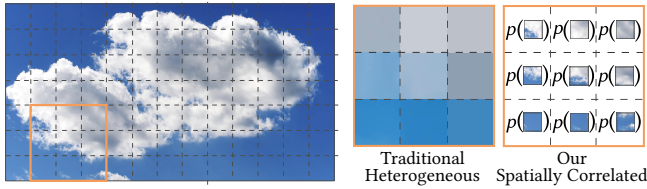


Fig. 3. Difference between heterogeneous and spatially-correlated media, from a computer graphics perspective. Heterogeneous media assume heterogeneity at macroscopic level, but local homogeneity at each differential volume $dV(\mathbf{x})$ (see “Traditional Heterogeneous”, represented as solid colors per voxel). Instead, our model for spatially-correlated media takes into account the uneven distribution of scatterers within each $dV(\mathbf{x})$ (represented on the right as probabilities of extinction $p(\cdot)$).

but omitted the underlying theory, and did not relate their model with the physical process of extinction. More formally, d’Eon analyzed rigorously the effect of isotropic non-Poissonian extinction on the diffusion (multiple scattering) regime [2014b; 2016a], and discussed the connections between graphics and non-classical transport, including the limitations of such theories to be used in rendering [d’Eon 2014a, 2016b]. We generalize these works, offering a non-classic transport theory suitable for rendering, and introduce an intuitive formulation for rendering spatially-correlated media based on local optical parameters.

3 RADIATIVE TRANSPORT IN CORRELATED MEDIA

In this section, we first introduce light transport in participating media as modeled by the Radiative Transfer Equation (RTE) [Chandrasekhar 1960] (Section 3.1). We then describe the notion of spatial correlation in media, and its effect on light extinction (Section 3.2), as well as the Generalized Boltzmann Equation (GBE), first proposed by Larsen [2007] in the context of neutron transport (Section 3.3).

It is important to first clarify the difference between spatially-correlated media, and heterogeneous media, as commonly used in computer graphics. As illustrated in Figure 3, heterogeneous media assume *local* homogeneity at each differential volume $dV(\mathbf{x})$. In contrast, correlated media take into account the average effect of uneven scatterer distributions within each $dV(\mathbf{x})$. Therefore, a medium can be *statistically homogeneous*, meaning that its statistical moments are invariant over all the volume, but spatially correlated [Kostinski 2001].

3.1 Background: The Radiative Transport Equation

In its integro-differential form, the Radiative Transfer Equation (RTE) models the amount of radiance L at point \mathbf{x} in direction ω_o as:

$$\omega_o \cdot \nabla L(\mathbf{x}, \omega_o) + \mu L(\mathbf{x}, \omega_o) = S(\mathbf{x}, \omega_o) + Q(\mathbf{x}, \omega_o), \quad (1)$$

where $Q(\omega_o)$ is the volume source term, and S is the in-scattered radiance:

$$S(\mathbf{x}, \omega_o) = \mu_s \int_{\Omega} L(\mathbf{x}, \omega_i) f_r(\mathbf{x}, \omega_i, \omega_o) d\omega_i, \quad (2)$$

which is the directional integral over the sphere Ω of the light scattered towards ω_o , modeled using the phase function f_r ; ω_i represents the incoming direction of light. Note that we have omitted

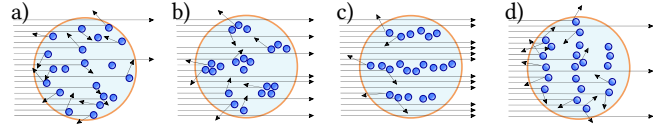


Fig. 4. Illustration of the effect of spatial correlation in a medium for different hypothetical distributions of scatterers. (a) A random distribution of scatterers within a differential volume $dV(\mathbf{x})$. (b) In the presence of scatterer correlation, the probability of interaction changes within $dV(\mathbf{x})$. (c, d) This correlation might further exhibit directional behavior, leading to very different interaction probabilities according to the degree of alignment with the propagation of light.

the spatial dependency of all terms in Equations (1) and (2) for simplicity. Finally, $\mu = \mu_a + \mu_s$ [m^{-1}] is the extinction coefficient, with μ_a and μ_s the absorption and scattering coefficients respectively. These terms model the probability of a beam of light to be attenuated either by absorption or scattering, and are defined as the product of the number of scatterers per unit volume C [m^{-3}], and the scatterers’ cross section σ [m^2], assuming that the scatterers are uniformly distributed in the differential volume (Figure 1, left) (see [Arvo 1993] for a detailed derivation). Jakob et al. [2010] later generalized the RTE to model directionally anisotropic media, by taking into account the angular (directional) dependence of the scatterers’s cross section in media.

3.2 Effect of Spatial Correlation on Extinction

When light propagates through a participating medium, it scatters as a function of the distribution of the scatterers. When this distribution is random and uniformly distributed, extinction becomes a Poissonian process, and the exponential Beer-Lambert law accurately describes the attenuation of light (see [Gallavotti 1972] for a rigorous derivation). However, the distribution of scatterers in many media exhibit different forms and degrees of spatial correlation (e.g. clouds [Davis and Marshak 2004; Lovejoy et al. 1995], textiles [Coquard and Baillis 2006], porous materials [Bellet et al. 2009; Taine et al. 2010], or granular aggregates [Meng et al. 2015]). This affects light transport, as Figure 4 illustrates; as a consequence, attenuation is no longer exponential, and light extinction becomes non-Poissonian.

Negative correlation occurs when the distribution of scatterers is more uniform than Poisson (as in electrostatic repulsion), and leads to super-exponential (faster) extinction. Clustered scatterers, on the other hand, yield positive correlation, which leads to sub-exponential (slower) extinction; this is illustrated in Figure 5. The reason for such non-exponential transmittance can be further visualized intuitively in Figure 6: In negatively-correlated media, absorbers are less likely to “shadow” one another; as a result, more light becomes extinct. Positively-correlated media presents the opposite case, with many absorbers shadowing others; this creates empty regions which in turn lead to more light passing through.

More formally, in uncorrelated media (Poissonian process) the extinction probability after traveling a distance t from the previous scattering (or emission²) event is $p(t) = \mu \exp(-\mu t)$, as predicted

²We will refer only to scattering events from now on for simplicity.

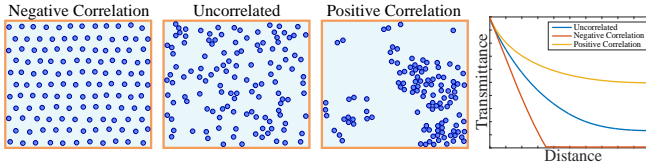


Fig. 5. Different types of scatterer correlation, and their effect on transmittance. From left to right, the first three figures depict negative correlation, no correlation (extinction is a Poissonian process), and positive correlation. The plot on the right shows extinction, averaged for several procedural realizations of the media (see Section S.13) and ray directions: While uncorrelated media results in the classic exponential extinction, negative and positive correlation lead to faster- and slower-than-exponential extinction, respectively.

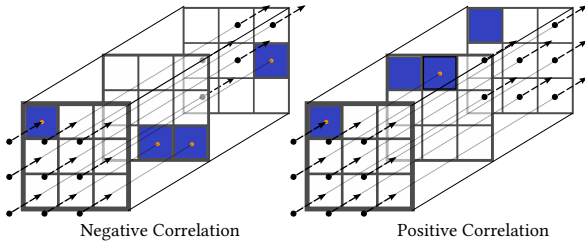


Fig. 6. Intuitive explanation for non-exponential transmittance in negatively- (left) and positively-correlated (right) media. Solid squares represent perfect absorbers. Although both media have the same number of absorbers, shadowing (or overlapping) of such scatterers (positive correlation) results in less (sub-exponential) extinction. Figure inspired from [Kostinski 2002].

by the Beer-Lambert law. Thus, defining the differential probability of extinction $\Sigma(t)$ [m^{-1}] as [Larsen and Vasques 2011]

$$\Sigma(t) = \frac{p(t)}{1 - \int_0^t p(s) ds}, \quad (3)$$

where the denominator is the physical definition of transmittance $T(t)$, we obtain $\Sigma(t) = \mu$, the extinction coefficient of the media (uniform for each differential volume, and independent of the distance t).

Let us now define a simple positively correlated (clustered) medium, composed of regions with a high density of scatterers (extinction coefficient μ_1), and regions with low density (μ_2). The probability of light extinction³ after traveling a distance t is given by

$$p(t) = \mu_1 p_\tau(\mu_1) e^{-\mu_1 t} + \mu_2 p_\tau(\mu_2) e^{-\mu_2 t}, \quad (4)$$

with $p_\tau(\mu_1)$ and $p_\tau(\mu_2)$ the probability of traversing a region with extinction coefficients μ_1 and μ_2 respectively, where $p_\tau(\mu_1) + p_\tau(\mu_2) = 1$. From this simple example, we can see that $p(t)$ is no longer exponential, and thus extinction is no longer a Poissonian process with a constant $\Sigma(t) = \mu$. Instead, plugging Equation (4) into Equation (3) leads to a function dependent on t . In other words, spatial correlation introduces a *memory effect* [Kostinski 2002], where the differential probability of extinction depends on the traveled distance t since the previous scattering event. This has a significant

³The probability of extinction $p(t)$ is also termed in the literature as “path length distribution”, “free path distribution”, or “chord length distribution”.

effect in the final volumetric appearance of the medium, as shown in Figure 1 and throughout this paper.

3.3 The Generalized Boltzmann Equation

Since $\Sigma(t)$ is a function of t in the presence of correlation, we need to introduce the t -dependent flux $L(\mathbf{x}, \omega_o, t)$ [$\text{W m}^{-2} \text{sr}^{-1} \text{m}^{-1}$], the flux at \mathbf{x} after traveling a distance t from the last scattering event. It relates with classic flux $L(\mathbf{x}, \omega_o)$ [$\text{W m}^{-2} \text{sr}^{-1}$] as $L(\mathbf{x}, \omega_o) = \int_0^\infty L(\mathbf{x}, \omega_o, t) dt$, and in turn introduces an additional derivative term in Equation (1), resulting in the Generalized Boltzmann Equation [Larsen 2007; Larsen and Vasques 2011]:

$$\begin{aligned} \frac{d}{dt} L(\mathbf{x}, \omega_o, t) + \omega_o \cdot \nabla L(\mathbf{x}, \omega_o, t) + \Sigma(t) L(\mathbf{x}, \omega_o, t) &= 0, \\ L(\mathbf{x}, \omega_o, 0) &= \underbrace{\int_0^\infty \Sigma_s(t) \int_\Omega L(\mathbf{x}, \omega_i, t) f_r(\omega_i, \omega_o) d\omega_i dt}_{\text{Inscattering } S(\mathbf{x}, \omega_o)} + Q(\mathbf{x}, \omega_o), \end{aligned} \quad (5)$$

where $\Sigma_s(t) = \Lambda \Sigma(t)$ is the probability of a photon being scattered after traveling a distance t (see Section S.3 for the full derivation), and Λ represents albedo. The second line of the equation represents the value for $t = 0$, in which light is scattered or emitted. Thus, after each scattering event the memory effect for the extinction is reset to zero.

As expected, by removing the t -dependency as $\Sigma(t) = \Sigma$, and integrating Equation (5), we obtain the classic RTE [Equation (1)] (see Section S.4). Moreover, Equation (5) can also support directionally anisotropic media [Jakob et al. 2010] by formulating Σ as a function of ω_o [Vasques and Larsen 2014].

4 OUR EXTENDED GBE

4.1 Limitations of the GBE

Unfortunately, Equation (5) relies on a set of simplifying assumptions, which limit its applicability in rendering applications. In particular [Larsen 2007; Larsen and Vasques 2011]:⁴

- (1) The medium is statistically homogeneous, and infinite; no system boundaries exist.
- (2) The phase function $f_r(\omega_i, \omega_o)$ and albedo Λ are independent of t . For example, in a mixture of two types of scatterers with different phase function or albedo, this assumes that both types have the same structure.
- (3) The source term $Q(\mathbf{x}, \omega_o)$ is correlated with the scatterers in the volume. This assumption does not hold in most cases, as illustrated in Figure 7.

In order to make the GBE useful for rendering, we need to extend it beyond these limiting assumptions. We describe this in the rest of this section, introducing our novel Extended GBE.

4.2 Extending the GBE

To lift the first and second limitations of the standard GBE, we first reformulate Σ , Λ , and f_r as functions of the spatial position

⁴Larsen and Vasques also assume a monoenergetic system; for simplicity, we assume also a single wavelength, although removing this limitation is straight forward.

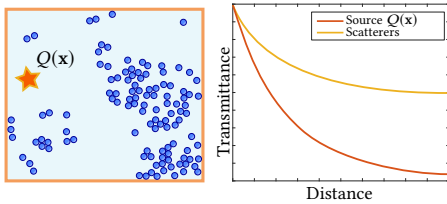


Fig. 7. Left: an uncorrelated light source $Q(\mathbf{x})$ in a positively correlated medium. The differential probability of extinction $\Sigma(\mathbf{x}, t)$ is therefore different for each, which significantly modifies light transport, as shown in the right, where transmittance is numerically computed from several procedurally generated media with identical positive correlation. This difference is not captured in Larsen’s original GBE [Larsen and Vasques 2011].

and the traveled distance, as $\Sigma(\mathbf{x}, t)$, $\Lambda(\mathbf{x}, t)$, and $f_r(\mathbf{x}, \omega_i, \omega_o, t)$ respectively. This means that, depending on the traveled distance t , light will be scattered differently, according to the different spatial correlation of the scatterers. Note that some previous works in graphics [Frisvad et al. 2007; Sadeghi et al. 2012] have included a mixture of scatterer sizes in the medium, but not spatial correlation. Defining the directional scattering operator $B(\mathbf{x}, \omega_i, \omega_o, t) = \Lambda(\mathbf{x}, t) \Sigma(\mathbf{x}, t) f_r(\mathbf{x}, \omega_i, \omega_o, t)$ for compactness, Equation (5) becomes

$$\begin{aligned} \frac{d}{dt} L(\mathbf{x}, \omega_o, t) + \omega_o \cdot \nabla L(\mathbf{x}, \omega_o, t) + \Sigma(t) L(\mathbf{x}, \omega_o, t) &= 0, \\ L(\mathbf{x}, \omega_o, 0) &= \int_0^\infty \int_\Omega L(\mathbf{x}, \omega_i, t) B(\mathbf{x}, \omega_i, \omega_o, t) d\omega_i dt + Q(\mathbf{x}, \omega_o), \end{aligned} \quad (6)$$

where we assume an isotropic formulation to avoid cluttering.

The third assumption, on the other hand, requires a more significant change of Equation (5). In Larsen’s original formulation of the GBE, since $L(\mathbf{x}, \omega_o, 0)$ includes both scattering $S(\mathbf{x}, \omega_o)$ and light emitted by sources $Q(\mathbf{x}, \omega_o)$, both terms implicitly share the same differential probability of extinction $\Sigma(\mathbf{x}, t)$. However, this would only be true if they present the exact same correlation (e.g. the scattering and the emissive particles are the same); in the general case, $\Sigma(\mathbf{x}, t)$ is different for S and Q . Moreover, different sources Q might correlate differently with the medium, leading to different $\Sigma(\mathbf{x}, t)$ per source. Figure 7 shows how different $\Sigma(\mathbf{x}, t)$ for scatterers and sources significantly affects light transport. This different correlation between sources and scatterers is in fact very important for rendering realistic scenes, since as we shown later in Section 4.3 reflection at media boundaries act as uncorrelated sources.

Taking all this into account, we can express radiance $L(\mathbf{x}, \omega_o, t)$ as

$$L(\mathbf{x}, \omega_o, t) = L_S(\mathbf{x}, \omega_o, t) + \sum_j L_{Q_j}(\mathbf{x}, \omega_o, t), \quad (7)$$

where $L_S(\mathbf{x}, \omega_o, t)$ is the *scattered* radiance reaching \mathbf{x} after traveling a distance t since the last scattering event, and $L_{Q_j}(\mathbf{x}, \omega_o, t)$ is the *unscattered* radiance directly emitted by source Q_j , which has traveled a distance t since emission. We can then transform Equation (6) into our Extended GBE as

$$\begin{aligned} \frac{d}{dt} L(\mathbf{x}, \omega_o, t) + \omega_o \cdot \nabla L(\mathbf{x}, \omega_o, t) + \Sigma_S(\mathbf{x}, t) L_S(\mathbf{x}, \omega_o, t) \\ + \sum_j \Sigma_{Q_j}(\mathbf{x}, t) L_{Q_j}(\mathbf{x}, \omega_o, t) &= 0, \end{aligned} \quad (8)$$

where $\Sigma_S(\mathbf{x}, t)$ and $\Sigma_{Q_j}(\mathbf{x}, t)$ are the differential extinction probabilities for the scattered photons and the (unscattered) photons emitted by light source Q_j , respectively. Then, for $t = 0$ we have

$$\begin{aligned} L_S(\mathbf{x}, \omega_o, 0) &= \int_0^\infty \int_\Omega \left(B_S(\mathbf{x}, \omega_i, \omega_o, t) L_S(\mathbf{x}, \omega_i, t) \right. \\ &\quad \left. + \sum_j B_{Q_j}(\mathbf{x}, \omega_i, \omega_o, t) L_{Q_j}(\mathbf{x}, \omega_i, t) \right) d\omega_i dt, \\ L_{Q_j}(\mathbf{x}, \omega_o, 0) &= Q_j(\mathbf{x}, \omega_o), \end{aligned} \quad (9)$$

where $B_S(\mathbf{x}, \omega_i, \omega_o, t) = \Lambda_S(\mathbf{x}, t) \Sigma_S(\mathbf{x}, t) f_{r,S}(\mathbf{x}, \omega_i, \omega_o, t)$ is the scattering operator for scattered photons (thus representing a *multiple scattering* operator), and $B_{Q_j}(\mathbf{x}, \omega_i, \omega_o, t)$ is the scattering operator for photons emitted by light source Q_j (*single scattering* operator). Note how, interestingly, Equation (9) makes the convenient separation between multiple and single scattering explicit. Similar to $\Sigma(\mathbf{x}, t)$, the phase function and albedo terms might also be different, depending on the correlation between sources and the scatterers. It is easy to verify that when the sources and scatterers are equally correlated with the rest of the medium, the Extended GBE in Equation (8) simplifies to Equation (5) (see Section S.5).

Integral form of the Extended GBE In order to get an integral formulation of our Extended GBE usable in a general Monte Carlo renderer, we solve Equation (8) for the incoming radiance at point \mathbf{x} as (see Section S.6 for the full derivation):

$$\begin{aligned} L(\mathbf{x}, \omega_o) &= \int_0^\infty T_S(\mathbf{x}, \mathbf{x}_t) S(\mathbf{x}_t, \omega_o) \\ &\quad + \sum_j \int_0^\infty T_{Q_j}(\mathbf{x}, \mathbf{x}_t) Q_j(\mathbf{x}_t, \omega_o) dt, \end{aligned} \quad (10)$$

where $\mathbf{x}_t = \mathbf{x} - \omega_o t$. The terms $T_S(\mathbf{x}, \mathbf{x}_t) = e^{-\int_0^t \Sigma_S(\mathbf{x}, s) ds}$ and $T_{Q_j}(\mathbf{x}, \mathbf{x}_t) = e^{-\int_0^t \Sigma_{Q_j}(\mathbf{x}, s) ds}$ represent transmittance between \mathbf{x} and \mathbf{x}_t for the scattered and emitted radiance, respectively. Last, $S(\mathbf{x}_t, \omega_o)$ is

$$\begin{aligned} S(\mathbf{x}_t, \omega_o) &= \int_0^\infty \int_\Omega \left(B_S(\mathbf{x}_t', \omega_i, \omega_o, t') S(\mathbf{x}_t', \omega_i) T_S(\mathbf{x}_t, \mathbf{x}_t') \right. \\ &\quad \left. + \sum_j B_{Q_j}(\mathbf{x}_t', \omega_i, \omega_o, t') Q_j(\mathbf{x}_t', \omega_o) T_{Q_j}(\mathbf{x}_t, \mathbf{x}_t') \right) d\omega_i dt', \end{aligned} \quad (11)$$

where $\mathbf{x}_t' = \mathbf{x}_t + \omega_i t'$. Next, we describe boundary conditions, and how they affect light transport.

4.3 Boundary Conditions

The assumption that the medium is infinite and homogeneous ignores changes in correlation that occur at boundaries, such as photons entering a medium, the presence of surfaces inside, or the

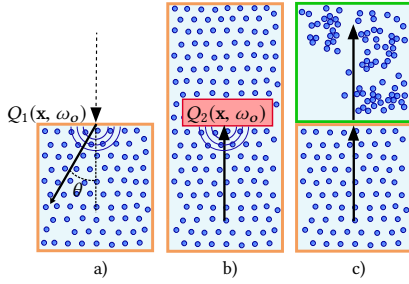


Fig. 8. Schematic example of the different boundary conditions: a) light entering a medium (*Vacuum to Medium*); b) light being reflected from a boundary back into the medium (*Medium to Surface*); and c) light crossing the interface between two different media (*Medium to Medium*). Refer to the text for details.

interface between two different media. Figure 8 illustrates the different boundary conditions and their effects in light transport. Here, we describe them and show how to incorporate them to our model.

Vacuum to Medium (Figure 8a): This is the simplest case, where an *uncorrelated* photon (from an uncorrelated medium or the vacuum) enters a correlated medium. It can be modeled as a source $Q_1(\mathbf{x}, \omega_o)$ at the entry boundary point \mathbf{x} , with $t = 0$.

Medium to Surface (Figure 8b): This case accounts for the interaction with surfaces such as a dielectric boundary, or an object placed inside the medium. Such surfaces are uncorrelated with respect to the medium. We can model this as a new source $Q_2(\mathbf{x}, \omega_o) = L_S(\mathbf{x}, \omega_i)f(\mathbf{x}, \omega_i, \omega_o)$, with $L_S(\mathbf{x}, \omega_i)$ and $f(\mathbf{x}, \omega_i, \omega_o)$ the incoming radiance at \mathbf{x} and the BSDF respectively, and setting $t = 0$.

Medium to Medium (Figure 8c): A photon crosses the interface between two different homogeneous media of different structure and correlation (this boundary condition therefore enables modeling heterogeneous media as well). The probability of extinction in the second medium $p_2(t)$ depends not only on its correlation η_2 and the correlation of the first medium η_1 , but also on the correlation *between the two media* $\eta_{1,2}$.

Figure 9 shows results for all three boundary conditions; please refer to Section S.13.3 for a more exhaustive set of examples.

5 RENDERING WITH THE EXTENDED GBE

Up to this point, we have extended Larsen’s original GBE formulation [Equation (5)], lifting the assumptions that made it unsuitable for rendering, presenting it also in integral form. Our Extended GBE [Equations (8) and (11)] supports an arbitrary mixture of scatterers (see Appendix S.1), and accounts for the effect of different correlation between scatterers and sources. To use it for rendering, the required differential extinction probabilities can be tabulated [Frank and Goudon 2010; Larsen and Vasques 2011] by simulating via Monte Carlo an estimate of $p(t)$, based on an explicit representation of the volume. This is a similar approach to our numerical results in Section S.13, and the validation curves computed by Meng et al. [2015, Figure 6] to validate their uncorrelated radiative transfer-based approximation. Alternatively, and empirical $p(t)$ can be used, fitting the observed transmittance in experimental setups, as is common

in atmospheric sciences [Davis et al. 1999]. In both cases, $\Sigma(\mathbf{x}, t)$ is computed by inverting $p(t)$ via Equation (3).

In computer graphics, participating media are usually described in terms of their optical parameters. However, in our current formulation of the Extended GBE, there is no explicit connection with such parameters. In the following, we provide the missing connection: We formulate a model for correlated media based on the optical parameters commonly used in rendering, which is intuitive to use and easy to plug into our Extended GBE. Then, we propose a simplified version of the model based on the assumption of positive correlation, which is easy to use and efficient to sample and evaluate.

5.1 Modeling Correlated Media from Optical Parameters

In a rendering context, the optical properties of a participating medium (e.g. extinction coefficients, scattering albedo, or phase function) are usually defined locally. Unfortunately, at the heart of our Extended GBE [Equation (8)] lies the differential extinction probability $\Sigma(\mathbf{x}, t)$, whose *memory effect* depends on the spatial correlation at neighboring points, and thus cannot be defined locally. Our goal then is to model $\Sigma(\mathbf{x}, t)$ and its derived quantities $p(t)$ and $T(t)$, based on probability distributions of extinction $p_\tau(\mu)$. In the following, we assume both homogeneity in the neighborhood of \mathbf{x} and isotropy, so we remove the spatial and angular dependence from the following derivations for clarity.

Given a ray \mathbf{r} in a medium, we can define its input radiance as $L_i(\mathbf{r})$, and its attenuation as $\mathcal{T}(\tau_t(\mathbf{r}))$, the ratio of input and output radiance of a single ray \mathbf{r} defined as a probabilistic function, which depends on the ray’s optical depth $\tau_t(\mathbf{r})$. Considering now a beam of light \mathcal{R} composed of several parallel rays $\mathbf{r} \in \mathcal{R}$ (see Figure 10), the total radiance $L_o(t)$ traveling a distance t in a correlated medium can be expressed as

$$L_o(t) = \int_{\mathcal{R}} L_i(\mathbf{r}) \mathcal{T}(\tau_t(\mathbf{r})) d\mathbf{r}. \quad (13)$$

In granular media [Moon et al. 2007], where the correlation length is larger than a differential distance dt (and usually larger than the granular particle’s size), the probability of extinction $p(t)$ depends on the distribution of scatterers along the direction of propagation of light, and needs to be taken into account explicitly. However, local correlation is assumed to be smaller than dt ; this means that the exact position of the scatterers within the volume becomes irrelevant, and only their projection onto the plane \mathcal{P} perpendicular to the propagation direction beam \mathcal{R} matters. We can then simplify the expression for the optical depth⁵ to the homogeneous case where $\tau_t(\mathbf{r}) = \mu(\mathbf{r})t$, with $\mu(\mathbf{r})$ the density of scatterers found by an individual ray \mathbf{r} when traversing the medium.

However, explicitly integrating over all rays in \mathcal{R} is not practical. Instead, we would like to find a compact way of relating $L_i(\mathbf{r})$ to the extinction coefficient $\mu(\mathbf{r})$. We can remove its dependence on ray \mathbf{r} by modeling L_i as a probability distribution $p_L(L_i)$ (e.g. by taking the histogram of $L_i(\mathbf{r})$), and explicitly relating it with the extinction coefficient μ via a conditional probability distribution $p_\tau(\mu; L_i)$. We

⁵“Optical depth” is a standard term in physics, defined as the natural logarithm of the ratio of incident to transmitted radiant power through a material

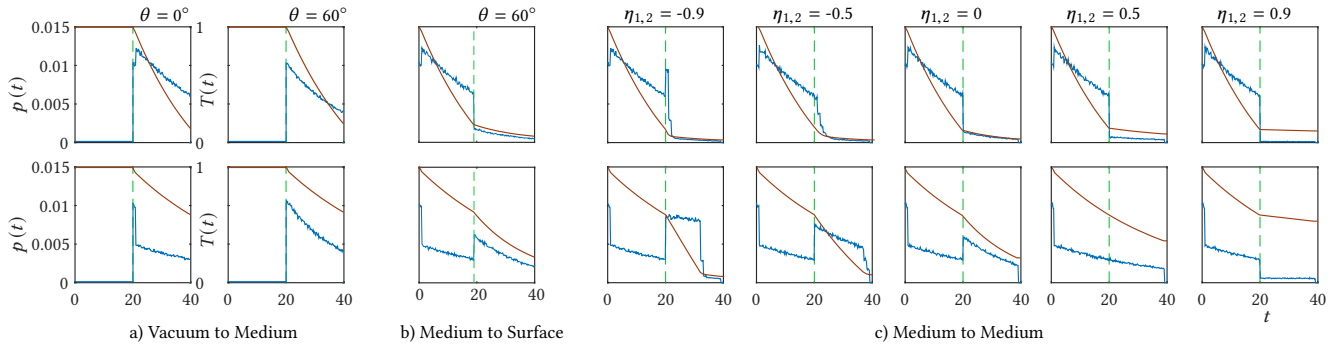


Fig. 9. Probability of extinction $p(t)$ (blue) and transmittance $T(t)$ (orange) as a function of t , for example cases of our three different boundary conditions. The vertical dotted line indicates the boundary. The first medium has a negative correlation $\eta_1 = -0.5$ on the top row, and positive $\eta_1 = 0.5$ on the bottom. (a) Vacuum to medium. When light enters the medium, it acts as a source term $Q(\mathbf{x}, \omega_o)$, which depends on the angle of incidence θ , since correlation might present some directionality (see Figure 8). (b) Medium to surface. As light is reflected on a surface boundary and changes direction, it acts as a directionally-resolved source $Q(\mathbf{x}, \omega_o)$ which depends on the surface BSDF. (c) Medium to medium, for a varying correlation $\eta_{1,2} = [-0.9, 0.9]$ between the two media. For increasingly positive correlation $\eta_{1,2}$ (high probability of the first medium shadowing the second), $p_2(t)$ becomes lower. For increasingly negative correlation $\eta_{1,2}$ (low shadowing probability), $p_2(t)$ becomes higher near the boundary (then depends on η_2). For uncorrelated media ($\eta_{1,2} = 0$), incoming photons can be modeled as sources at the entry boundary points, with $Q(\mathbf{x}, \omega_o)$ dependent on the correlation of the second medium η_2 . For all cases modeled as light sources $Q(\mathbf{x}, \omega_o)$, t is set to 0. Refer to the supplemental material for a more comprehensive set of examples.

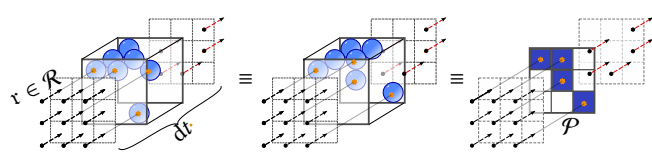


Fig. 10. Left and center: Examples of two differential volumes in a medium, each with different distribution of scatterers, but with a similar projection on the plane perpendicular to the direction of propagation (right).

therefore transform Equation (13) into

$$L_o(t) = \int_0^\infty \int_0^\infty p_L(L_i) p_\tau(\mu; L_i) L_i \mathcal{T}(\mu t) d\mu dL_i. \quad (14)$$

Defining $\hat{L}_i = \int_{\mathcal{R}} L_i(\mathbf{r}) d\mathbf{r} = \int_0^\infty p_L(L_i) L_i dL_i$, and using $T(t) = \frac{L_o(t)}{\hat{L}_i}$ we get

$$T(t) = \int_0^\infty \int_0^\infty p_L(L_i) p_\tau(\mu; L_i) \frac{L_i}{\hat{L}_i} \mathcal{T}(\mu t) d\mu dL_i, \quad (15)$$

which models transmittance $T(t)$ as a function of the correlation between the light and the distribution of local scatterers. Finally, from Equation (15) we can compute the probability of extinction as $p(t) = \left| \frac{dT(t)}{dt} \right|$, while $\Sigma(t)$ can be obtained as $\Sigma(t) = p(t)/T(t)$ [Equation (3)].

5.2 An intuitive local model for positively-correlated media

Equation (15) is general and can model any type of correlation; For the common case of positive correlation, we can set $\mathcal{T}(\mu t) = e^{-\mu t}$ (see [Kostinski 2002] for details), and assume that $p_L(L_i)$ and $p_\tau(\mu)$ are independent, so that $p_\tau(\mu; L_i) = p_\tau(\mu)$. We can then rewrite Equation (15) as (see Section S.7)

$$T(t) = \int_0^\infty e^{-\mu t} p_\tau(\mu) d\mu. \quad (16)$$

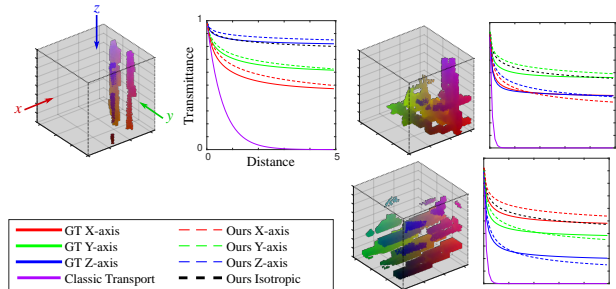


Fig. 11. Transmittance in high-resolution volumes of locally-correlated media (procedurally generated after [Lopez-Moreno et al. 2015]). Beams of light travel through each volume, aligned in succession to the x , y , and z axes. Ground-truth transmittance (red, green, and blue solid lines) has been computed by brute force regular tracking [Amanatides and Woo 1987], while our simulation (dotted lines) uses the gamma distribution proposed in Equation 19. Classic transport governed by the RTE significantly overestimates extinction through the volume, resulting in an exponential decay (purple line). In contrast, our model matches ground-truth transmission much more closely. The black dotted line is the result of isotropic correlation, which is clearly also non-exponential. Please refer to Figure S.24 in the supplemental for more examples.

Using again the relationship in Equation (3), we obtain the differential extinction probability

$$\Sigma(t) = \frac{p(t)}{T(t)} = \frac{\int_0^\infty \mu e^{-\mu t} p_\tau(\mu) d\mu}{\int_0^\infty e^{-\mu t} p_\tau(\mu) d\mu}. \quad (17)$$

Note that this form of $p(t)$ [numerator in Equation (17)] is a generalization of the simple example in Equation (4) for a mixture of two different extinction coefficients. Assuming that the light distribution $p_L(L_i)$ from both sources Q_j and scatterers S is uncorrelated with the scatterers distribution $p_\tau(\mu)$, then $\Sigma(t) = \Sigma_S(t) = \Sigma_{Q_j}(t)$.

Finding a good distribution $p_\tau(\mu)$ To be able to use Equations (16) and (17), we need to find a good optical depth distribution $p_\tau(\mu)$ for the medium. Taking the average scatterers' cross section σ , we can define

$$\mu p_\tau(\mu) = C p_C(C) \sigma, \quad (18)$$

where C is the scatterers concentration and $p_C(C)$ its probability distribution. To find a practical $p_C(C)$ we analyzed a wide range of high-resolution volumes exhibiting different correlation (see Figure 11 for some examples). We observed that a gamma distribution fits $p_C(C)$ reasonably well, so that

$$p_C(C) \approx \Gamma(C; \alpha, \beta) = \frac{\beta^\alpha C^{\alpha-1} e^{-C\beta}}{\gamma(\alpha)}, \quad (19)$$

with $\alpha = \bar{C}^2 \cdot \text{Var}(C)^{-1}$, $\beta = \bar{C} \cdot \text{Var}(C)^{-1}$, and $\gamma(\alpha)$ the gamma function. Moreover, previous research has shown that the gamma distribution is also very adequate for modeling the concentration of turbulent media such as clouds [Barker et al. 1996], or particulate media [Peltoniemi and Lumme 1992].

Equation (19) provides a compact and intuitive description of the statistical properties of $p_C(C)$ (and in turn of $p_\tau(\mu)$ in Equation (18)), by only using its mean \bar{C} and variance $\text{Var}(C)$ (intuitively, a higher variance indicates clusters of scatterers with gaps between them). In contrast, traditional (uncorrelated) media depend only on the mean concentration \bar{C} , and assume $\text{Var}(C) = 0$. For simplicity, we have assumed that both $p_C(C)$ and σ are isotropic. Appendix S.2 shows how to add directional dependencies as $p_C(C; \omega_o)$ and $\sigma(\omega_o)$.

Rendering Using Equations (19) and (16), and noting that the latter is related with the moment distribution function $M(t)$ of $p_C(C)$ as $T(t) = M(-\sigma t)$ [Davis and Xu 2014], we can compute the transmittance, probability of extinction, and differential probability of extinction as

$$T(t) = \left(1 + \frac{\sigma \cdot t}{\beta}\right)^{-\alpha}, \quad (20)$$

$$p(t) = \frac{\alpha \sigma}{\beta} \left(\frac{\sigma t}{\beta} + 1\right)^{-(1+\alpha)}, \quad (21)$$

$$\Sigma(t) = \sigma \frac{\alpha}{\beta} \left(1 + \frac{\sigma t}{\beta}\right)^{-1}. \quad (22)$$

In Figure 11 we analyze the performance of our analytic expression of transmittance for correlated media in Equation (20), against the exponential transmittance predicted by the Beer-Lambert law, and ground-truth transmittance computed by brute force regular tracking [Amanatides and Woo 1987]. Our model is much closer to the ground truth than the result of classic light transport, which significantly overestimates extinction through the volume. Figure 12 explores our closed-form of transmittance: As variance increases, the slower-than-exponential behavior becomes more pronounced, as observed by Davis and Mineev-Weinstein [2011] when analyzing the frequency of density fluctuations in correlated media. This effect is not captured by classic light transport.

In a Monte Carlo renderer, we can compute a random walk by sampling transmittance using the probability defined in Equation (21). However, as opposed to the classic exponential transmittance in Beer-Lambert law, $p(t)$ is not proportional to $T(t)$, which may lead

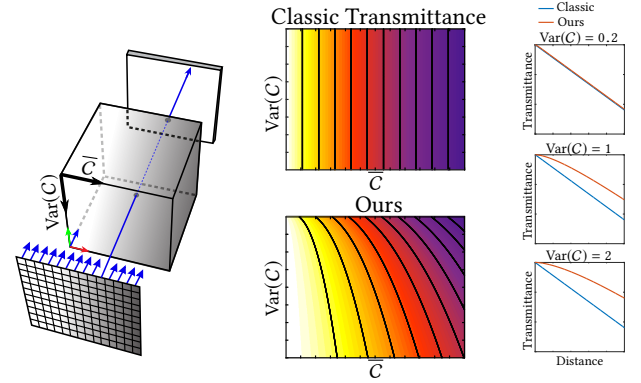


Fig. 12. Comparison between traditional transmittance as predicted by the Beer-Lambert law, and our transmittance for correlated media. The scene consists of a cube embedding a participating medium, placed in front of a light source. The media has a constant cross section $\sigma = 1$, and increasing scatterers concentration \bar{C} and correlation (i.e. density variance $\text{Var}(C)$) along the horizontal and vertical axes, respectively. Correlation does not affect transmittance in the classic model, which follows the Beer-Lambert law as shown in the log-scale plots on the right. In contrast, our model captures the slower-than-exponential decay as variance $\text{Var}(C)$ increases. We use $\bar{C} = 1$ for the plots. Figure after [Novák et al. 2014].

to increase variance of the estimate. To sample with a probability $p(t) \propto T(t)$, assuming $\alpha > 1$ (i.e. $\bar{C} > \sqrt{\text{Var}(C)}$) we can define $p(t)$ as

$$p(t) = -\sigma \frac{1-\alpha}{\beta} \left(1 + \frac{\sigma t}{\beta}\right)^{-\alpha} = -\sigma \frac{1-\alpha}{\beta} T(t), \quad (23)$$

which can be sampled using its inverse cdf

$$t(\xi) = -\frac{\beta}{\sigma} \left(1 - \sqrt[1-\alpha]{1-\xi}\right), \quad (24)$$

with $\xi \in [0, 1]$ a uniform random value. When the sampled distance t is longer than the distance t' to a boundary condition, the probability of an intersection at t' becomes

$$p(t') = \left(1 + \frac{\sigma t'}{\beta}\right)^{1-\alpha}. \quad (25)$$

We refer to Section S.9 for more detailed derivations, including the general case where $\alpha \leq 1$.

Implementation While correlated media can be implemented as a volumetric definition in most renderers, there are a few details that need to be taken into account. The most important one is that the constants used when solving the classic RTE (e.g. Λ or $\Sigma(t) = \mu$) are now defined as a function of t . As such, most of the optimizations typically done in the photon's random walk due to terms cancellation cannot be directly applied here. Additionally, the different correlations between scatterers and sources in Equation (11) require keeping track on the previous vertex of the path when sampling a new one (via selecting either $p_Q(t)$ or $p_S(t)$). This is also important when connecting with the light source via next-event estimation, where the source's transmittance and differential scattering probability need to be applied.

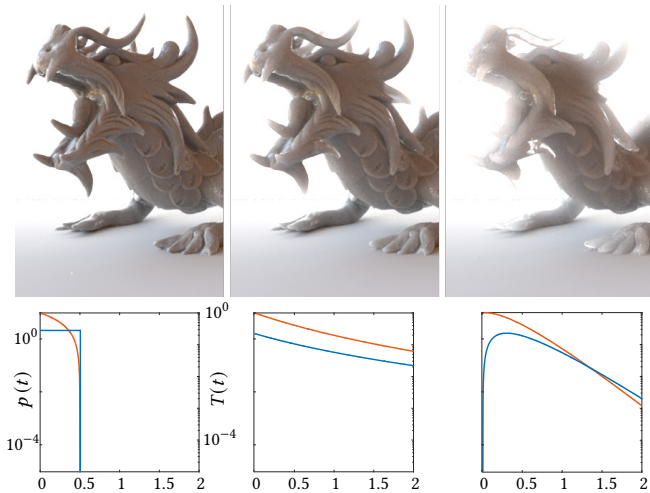


Fig. 13. Materials with different types of probability distributions of extinction $p(t)$ (shown in the bottom plots in blue, while transmittance $T(t)$ is shown in orange; both cases are in log-scale). From left to right: Negative correlation with linear extinction; a power-law $p(t)$ resulting from our local model (Section 5.2), with $\text{Var}(C(x)) = 1$; and an example of one empirical $p(t)$ following a gamma distribution with $\text{Var}(t) = .1$ (see Section S.10 for details). In all cases the mean extinction $\bar{\mu} = 2 \text{ m}^{-1}$, albedo $\Lambda = .8$, and isotropic phase function.

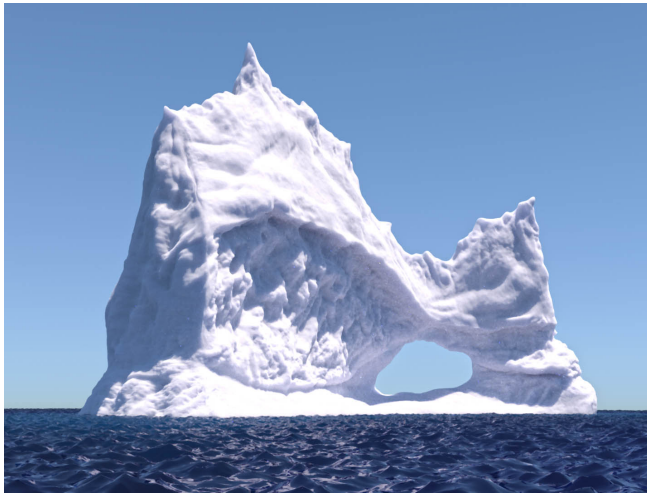


Fig. 14. Rendering of an iceberg made of compacted snow (with snow’s spectral cross section σ and albedo Λ after Frisvad and colleagues [2007]), using our model in Section 5.2.

6 RESULTS

In this section we show results using our new model for spatially-correlated participating media, including comparisons against the traditional RTE. We have implemented the integral form of our Extended GBE [Equation (11)] as a volumetric definition in Mitsuba [Jakob 2010]. For materials with negative correlation we have used a linear transmittance decay (see Section S.10 for details); for

| Figure | # Samples | Uncorrelated | Correlated |
|--------|-----------|--------------|-------------|
| 1 | 4096 | 53 m | 45 m / 58 m |
| 13 | 4096 | 30 m | 33 m / 35 m |
| 14 | 2048 | 185 m | 213 m |
| 15 | 4096 | 26 m | 28 m |
| 16 | 2048 | 5.6 m | 5.8 m |
| 17 | 8192 | 70 m | 82 m |
| 18 | 4096 | 17.71 m | 18.8 m |

Table 1. Computational cost for the images shown in the paper, for both uncorrelated (traditional model) and correlated media (ours). When different types of correlation are used, we show two measurements (positive / negative).

positive correlation, we used our local model in Section 5.2. Unless stated otherwise, we assume positively correlated media in our results. All our tests were performed on an Intel Core i7-6700K at 4GHz with 16 GB of RAM.

The cost introduced by sampling and evaluating the correlated transmittance with respect to classical transmittance is negligible in comparison to the cost of tracing samples. Simulation parameters and timings are shown in Table 1; note that negatively correlated media tend to create longer paths, therefore increasing the total rendering cost. In terms of convergence, in some cases the pdf might not be proportional to the sampled transmittance [e.g. in Equation (25)], which in turn might increase variance, we did not observe a strong effect when incorporating non-exponential transport. In Section S.12 we analyze the convergence experimentally.

Figure 1 shows volumetric renderings of translucent dragons made of materials with the same density, but different correlation. The middle image shows positive correlation, following a gamma distribution with $\text{Var}(C) = 40$. On the right we show negative correlation, exhibiting linear transmittance. In the three cases the media have scattering albedo $\Lambda = .8$, and mean extinction $\bar{\mu} = 10 \text{ m}^{-1}$. The net effect, due to the faster-than-exponential (negative correlation) and slower-than-exponential transmittance (positive correlation), is clearly visible in the final images.

Figure 13 highlights the versatility of our framework, with different scatterers correlation: negative correlation with linear transmittance decay, positive correlation according to our model, and an empirical distribution of $p(t)$ (modeled as a gamma distribution, see Section S.10). The mean extinction is in all cases $\bar{\mu} = 2 \text{ m}^{-1}$, with albedo $\Lambda = .8$. Both the particles concentration and the cross section are isotropic. Figure 14 shows another non-exponential probability of extinction on granular compacted snow, using our model in Section 5.2. Optical parameters of the snow have been computed after Frisvad et al. [2007].

In Figure 15 we analyze the effect of correlation with increasing variance [increasing $\text{Var}(C)$ in Equation (19)]. The top half of the jars has been rendered with the classic RTE, and thus remain constant independent of the degree of correlation, as expected. The bottom half shows the result of our model; note that for $\text{Var}(C) = 0$ the result converges with classic light transport.

Figure 16 shows the effect of directional correlation. The scene is made up of a volumetric prism with very low scattering albedo,

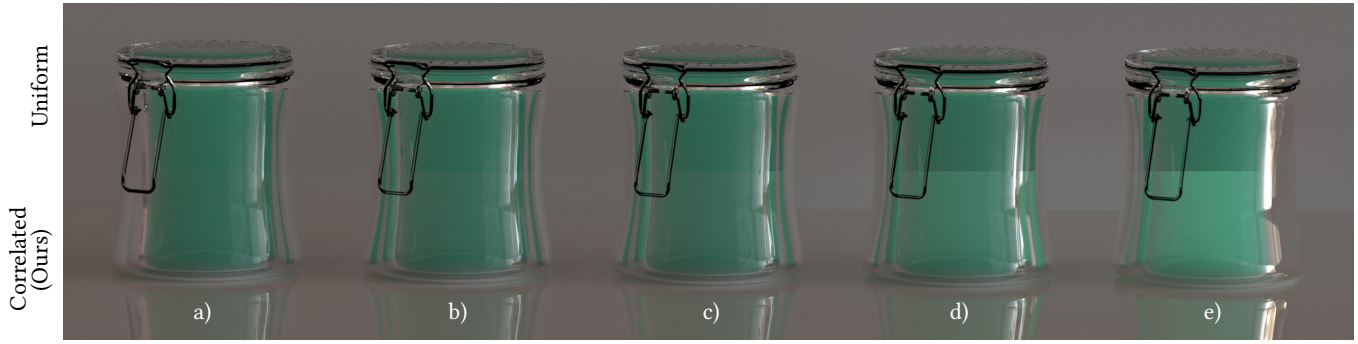


Fig. 15. Effect of local correlation in media with mean extinction of $\bar{\mu} = 2$ and albedo $\Lambda = \{.1, .8, .6\}$, and increasing variance $\text{Var}(C(x))$: a) 0, b) 8, c) 12, d) 16, and e) 32. The top half shows the result of classic light transport, while the bottom half shows the result of our model. For $\text{Var}(C(x)) = 0$ the result is identical to classic light transport.

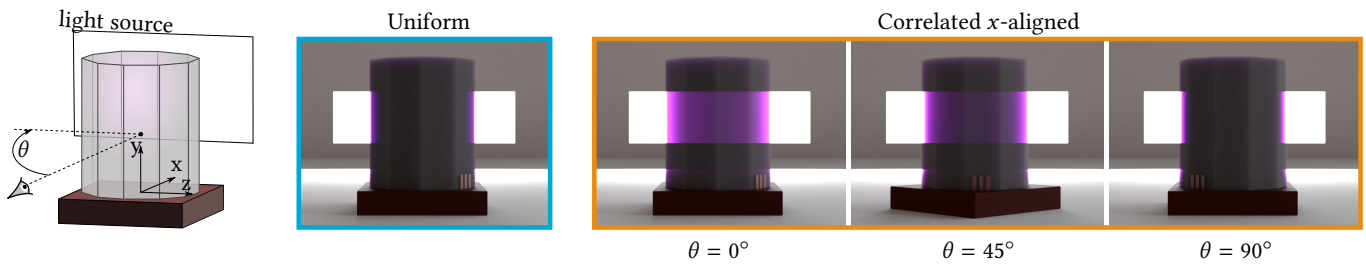


Fig. 16. Effect of directionally-dependent correlation on transmittance. The prism rotates around the y -axis. With uncorrelated media, appearance does not change with rotation. With a highly-correlated medium, appearance changes significantly as the prism rotates, according to the degree of alignment between the correlation and the view vector. The figure shows the case of x -axis-aligned correlation. Illustrative examples on the distribution of particles for each case are shown in Figure 4. Please refer to the supplemental for the video.

so the dominant effect is transmittance, and a strong rectangular area light placed behind it. The prism rotates around its y -axis. The first prism is made up of an uncorrelated medium, while the other three show a strong positive correlation along the x -axis, with $\text{Var}(C) = .5$; when the rotation angle is $\theta = 0^\circ$, correlation is perfectly aligned with the x -axis [similar to the situation depicted in Figure 4 (c)]. Both uncorrelated and correlated media have a mean particles concentration $\bar{C} = \{.8, 1.6, .7\}$ (RGB), and a mean cross section $\bar{\sigma} = 1$. For the uncorrelated media, no changes occur in appearance as the prism rotates, as expected. For the x -aligned correlation, transmittance varies significantly as correlation progressively becomes unaligned with the view vector. We refer the reader to the supplemental video for the full animation, including other directions of correlation. Figure 17 systematically analyzes the effect of directional correlation for varying albedos Λ , including uncorrelated media, isotropic correlated media, and directionally correlated media aligned with the x and z axes (being y the up-vector). These four scenarios roughly correspond to the ones depicted in Figure 4.

Last, in Figure 18 we investigate if adjusting the optical parameters of an uncorrelated medium and using the classic RTE could produce the same results as our model for correlated media. In particular, we render the first statue with a correlated material (mean extinction $\bar{C} = 20$, isotropic phase function, and scattering albedo $\Lambda = .8, .1, .1$), and render an uncorrelated version adjusting

$\bar{C} = 45$, with the same phase function and scattering albedo. Although tweaking the parameters of the RTE can lead to an overall similar appearance, it cannot correctly reproduce the details due to the different extinction curves and diffusive behavior in both models (see also [d'Eon 2014b]).

7 CONCLUSIONS

We have introduced a novel framework to simulate light transport in spatially-correlated media, where the probability of extinction and transmittance no longer follow an exponential decay, as predicted by the Beer-Lambert law. We have presented the Extended Generalized Boltzmann Equation, lifting the main limiting assumptions of the original GBE, and making it suitable for rendering applications. Our framework supports multiple sources, mixtures of particles, and directional correlation. In addition, we have proposed an intuitive model based on local optical properties for the most common case of positive correlation, providing a close-form solution for transmittance, without the need for costly numerical simulation or precomputations, allowing to model $\Sigma(t)$ based on local definitions of μ . Interestingly, Davis and Xu [2014] empirically proposed a similar expression to this model for transmittance in clouds. However, the authors stated that an integro-differential counterpart of their formulation was yet unknown. Our Equation (17) links this form of transmittance with the GBE, which is in turn an integro-differential equation.

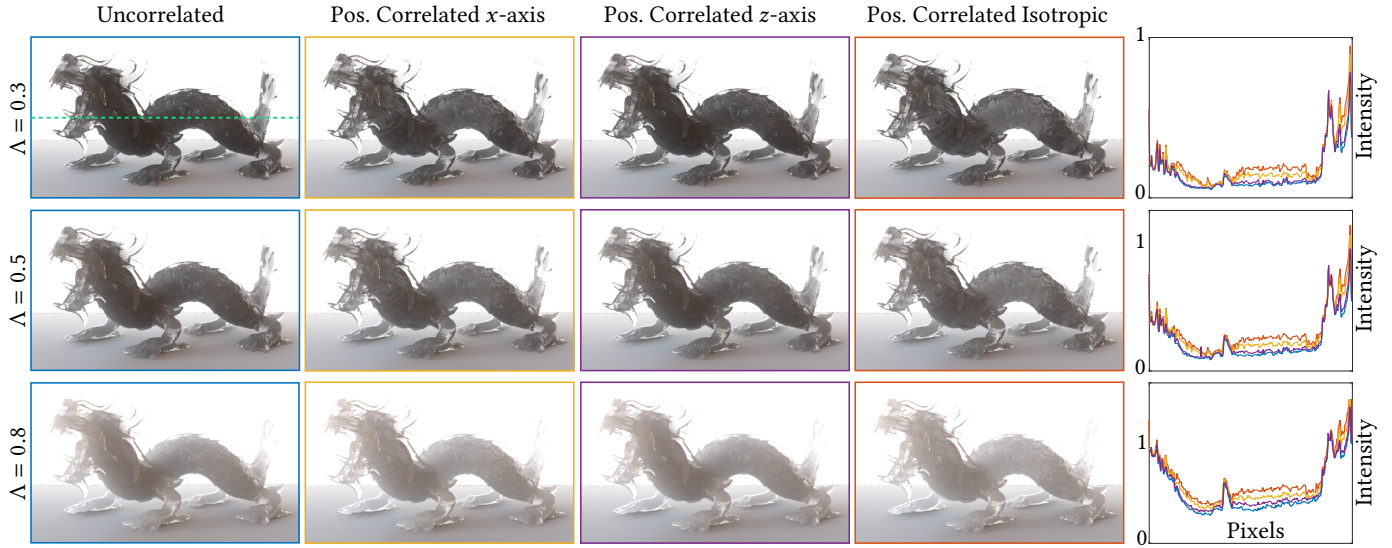


Fig. 17. Effect of directional correlation with varying albedos μ_s . From left to right: uniformly distributed media, directionally correlated in the x axis (aligned to the camera view), directionally correlated in z axis, and with isotropic correlation. For all cases we keep $\bar{C} = 10$, $\sigma = 1$, and $\text{Var}(C) = 10$ in the main axis of correlation, while for the remaining directions is close to zero (so the mean free path is similar to the predicted by Beer-Lambert law). To the right we plot intensity values (green scanline shown in one of the dragons) for each medium, showing the differences between classic light transport and our approach.

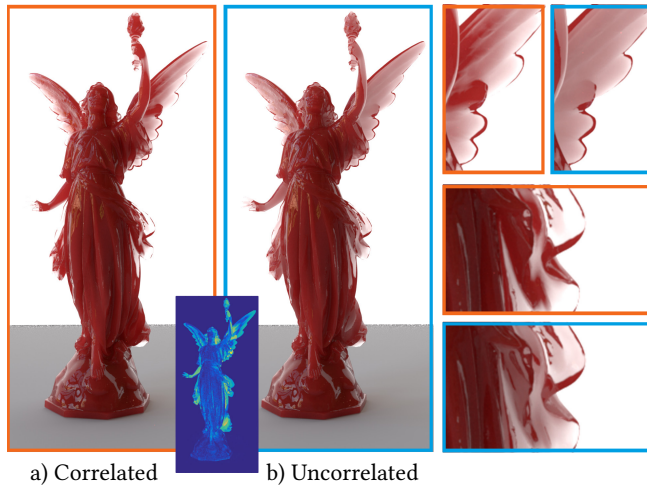


Fig. 18. Left: Render using our framework for correlated materials. Right: Render using the RTE, where the optical parameters of the material have been adjusted trying to match the appearance of the correlated case. Dissimilarities are evident, specially in thinner areas, since the extinction curves and diffusive behavior in both models are different (see false-color inset and zoomed-in areas).

Limitations and future work Our theoretical framework in Section 4 is general, and supports heterogeneous media through the medium-to-medium boundary condition. However, practical implementation of such heterogeneities for continuous media is still challenging. This is because the differential probability of extinction $\Sigma(\mathbf{x})$ at point \mathbf{x} affects $\Sigma(\mathbf{x} + \omega_o dt)$, according to the scatterers correlation at points \mathbf{x} and $\mathbf{x} + \omega_o dt$, and to the cross-correlation

between these two points. This means that the probability of extinction in correlated heterogeneous media cannot be modeled as the integral of the *local* differential extinction probabilities along the ray, as in uncorrelated heterogeneous media. In concurrent work, Camminady et al. [2017] proposed a solution for the simplest case, where the two media have identical structure $\eta_1 = \eta_2 = \eta_{1,2}$, and therefore the probability of extinction $p(t)$ only varies due to the different media density; however, finding an efficient, general solution remains a challenging problem. Revisiting numerical techniques for computing unbiased transmittance in heterogeneous media is thus an interesting topic of future work, since it is unclear how the underlying theory of virtual particles in existing methods [Coleman 1968; Kutz et al. 2017; Novák et al. 2014; Szirmay-Kalos et al. 2017; Woodcock et al. 1965] could be adapted to correlated scatterers. From a physical point of view, it would also be interesting to introduce in our Extended GBE [Equation (8)] support for refractive media [Ament et al. 2014; Gutierrez et al. 2006], as well as vector or bispectral scattering [Jarabo and Arellano 2018].

Other open problems include extending our local model [Equation (16)] to the case of negatively correlated media, thus removing precomputation or the definition of an empirical $p(t)$, or finding a model for the continuous transition between correlated and particulate media. While for perfect negative correlation we can model light-particle interactions as a Bernoulli process (see Section S.10.1), for other degrees of negative correlation this process is not obvious: We hypothesize that such cases could be modeled as a mixture of Poissonian and Bernoulli processes, although an analytical model for negative correlation remains an open challenge that deserves a more in-depth exploration. Finally, for our final model we have chosen a gamma distribution for $p_r(\mu)$; however other probability distributions might work better depending on the scenario. Moreover,

our directionally-resolved model for the variance of the distribution might be too smooth for materials with high-frequency details: in such cases, a mixture of ellipsoids (similar to the approach of Zhao et al. [2016]) could result in a more accurate fit.

Our definition of locally-correlated light transport may be suitable for filtering volumetric appearances, avoiding costly optimization procedures [Zhao et al. 2016], or ad-hoc shadowing functions [Schröder et al. 2011]. Accelerating rendering of particulate media [Meng et al. 2015; Müller et al. 2016] is another area that could benefit from our locally-correlated model. Introducing our compact representation into the shell transport functions proposed by Moon et al. [2007] and Müller et al. [2016] could significantly decrease the storage cost of these representations. Last, similarity theory [Wyman et al. 1989; Zhao et al. 2014] is an important tool for accelerating light transport within the RTE. Redefining this theory within locally-correlated radiative transport is another interesting avenue of work, specially given the additional degrees of freedom introduced by the non-exponential probability of extinction $p(t)$.

ACKNOWLEDGMENTS

We thank Miguel Angel Otaduy, Carlos Castillo and Jorge Lopez-Moreno for comments and discussions on early stages of the project and the dataset in Figure 11; Julio Marco, Adolfo Muñoz, and Ibón Guillén for discussions and proof-reading; Pilar Romeo for help with the figures; and the reviewers for the in-depth reviews. This project has been funded by the European Research Council (ERC) under the EU's Horizon 2020 research and innovation programme (project CHAMELEON, grant No 682080), DARPA (project REVEAL), and the Spanish Ministerio de Economía y Competitividad (projects TIN2016-78753-P and TIN2014-61696-EXP).

REFERENCES

- Carlos Aliaga, Carlos Castillo, Diego Gutierrez, Miguel A. Otaduy, Jorge Lopez-Moreno, and Adrian Jarabo. 2017. An Appearance Model for Textile Fibers. *Computer Graphics Forum (Proc. EGSR 2017)* 36, 4 (2017).
- John Amanatides and Andrew Woo. 1987. A fast voxel traversal algorithm for ray tracing. In *Eurographics*, Vol. 87. 3–10.
- Marco Ament, Christoph Bergmann, and Daniel Weiskopf. 2014. Refractive radiative transfer equation. *ACM Trans. Graph.* 33, 2 (2014).
- James Arvo. 1993. Transfer equations in global illumination. *SIGGRAPH '93 Course Notes* 2 (1993).
- Howard W Barker, Bruce A Wiellicki, and Lindsay Parker. 1996. A parameterization for computing grid-averaged solar fluxes for inhomogeneous marine boundary layer clouds. Part II: Validation using satellite data. *Journal of the Atmospheric Sciences* 53, 16 (1996).
- Fabien Bellet, Elie Chalopin, Florian Fichot, Estelle Iacona, and Jean Taine. 2009. RDFI determination of anisotropic and scattering dependent radiative conductivity tensors in porous media: Application to rod bundles. *International Journal of Heat and Mass Transfer* 52, 5 (2009), 1544–1551.
- Thomas Camminady, Martin Frank, and Edward W. Larsen. 2017. Nonclassical Particle Transport in Heterogeneous Materials. In *International Conference on Mathematics & Computational Methods Applied to Nuclear Science & Engineering*.
- Subrahmanyan Chandrasekhar. 1960. *Radiative Transfer*. Dover.
- WA Coleman. 1968. Mathematical verification of a certain Monte Carlo sampling technique and applications of the technique to radiation transport problems. *Nuclear science and engineering* 32, 1 (1968), 76–81.
- R Coquard and D Baillis. 2006. Radiative properties of dense fibrous medium containing fibers in the geometric limit. *Journal of heat transfer* 128, 10 (2006), 1022–1030.
- Anthony B Davis and Alexander Marshak. 2004. Photon propagation in heterogeneous optical media with spatial correlations: enhanced mean-free-paths and wider-than-exponential free-path distributions. *Journal of Quantitative Spectroscopy and Radiative Transfer* 84, 1 (2004).
- Anthony B Davis, Alexander Marshak, H Gerber, and Warren J Wiscombe. 1999. Horizontal structure of marine boundary layer clouds from centimeter to kilometer scales. *Journal of Geophysical Research: Atmospheres* 104, D6 (1999).
- Anthony B Davis and Mark B Mineev-Weinstein. 2011. Radiation propagation in random media: From positive to negative correlations in high-frequency fluctuations. *Journal of Quantitative Spectroscopy and Radiative Transfer* 112, 4 (2011).
- Anthony B Davis and Feng Xu. 2014. A Generalized Linear Transport Model for Spatially Correlated Stochastic Media. *Journal of Computational and Theoretical Transport* 43, 1-7 (2014).
- Eugene d'Eon. 2014a. Computer graphics and particle transport: our common heritage, recent cross-field parallels and the future of our rendering equation. In *Digipro 2014*.
- Eugene d'Eon. 2014b. Rigorous asymptotic and moment-preserving diffusion approximations for generalized linear Boltzmann transport in arbitrary dimension. *Transport Theory and Statistical Physics* 42, 6-7 (2014), 237–297.
- Eugene d'Eon. 2016a. *Diffusion approximations for nonclassical Boltzmann transport in arbitrary dimension*. Technical Report.
- Eugene d'Eon. 2016b. *A Hitchhiker's Guide to Multiple Scattering*.
- H. Scott Dumas, Laurent Dumas, and François Golse. 1996. On the mean free path for a periodic array of spherical obstacles. *Journal of statistical physics* 82, 5 (1996), 1385–1407.
- Martin Frank and Thierry Goudon. 2010. On a generalized Boltzmann equation for non-classical particle transport. *Kinetic and Related Models* 3 (2010).
- Jepp Revall Frisvad, Niels Jørgen Christensen, and Henrik Wann Jensen. 2007. Computing the scattering properties of participating media using Lorenz-Mie theory. *ACM Trans. Graph.* 26, 3 (2007).
- Giovanni Gallavotti. 1972. *Rigorous Theory Of The Boltzmann Equation In The Lorentz Gas*. Technical Report. Istituto di Fisica, Univ. di Roma.
- Diego Gutierrez, Adolfo Munoz, Oscar Anson, and Francisco Seron. 2006. Simulation of Atmospheric Phenomena. *Computers & Graphics* 30, 6 (2006), 994:1010.
- Diego Gutierrez, Srinivasa G. Narasimhan, Henrik Wann Jensen, and Wojciech Jarosz. 2008. Scattering. In *ACM SIGGRAPH ASIA 2008 Courses*.
- Eric Heitz, Jonathan Dupuy, Cyril Crassin, and Carsten Dachsbacher. 2015. The SGGX Microflake Distribution. *ACM Trans. Graph.* 34, 4, Article 48 (2015). <http://doi.acm.org/10.1145/2766988>
- Wenzel Jakob. 2010. Mitsuba renderer. (2010). <http://www.mitsuba-renderer.org>.
- Wenzel Jakob, Adam Arbree, Jonathan T Moon, Kavita Bala, and Steve Marschner. 2010. A radiative transfer framework for rendering materials with anisotropic structure. *ACM Trans. Graph.* 29, 4 (2010).
- Adrian Jarabo and Victor Arellano. 2018. Bidirectional Rendering of Vector Light Transport. *Computer Graphics Forum* To appear (2018).
- Wojciech Jarosz, Derek Nowrouzezahrai, Iman Sadeghi, and Henrik Wann Jensen. 2011. A Comprehensive Theory of Volumetric Radiance Estimation Using Photon Points and Beams. *ACM Trans. Graph.* 30, 1 (2011).
- Henrik Wann Jensen. 2001. *Realistic Image Synthesis Using Photon Mapping*. AK Peters.
- Pramook Khungurn, Daniel Schroeder, Shuang Zhao, Kavita Bala, and Steve Marschner. 2015. Matching Real Fabrics with Micro-Appearance Models. *ACM Trans. Graph.* 35, 1 (2015).
- Yuri Knyazikhin, Jörn Kranigk, Ranga B Myneni, Oleg Panforyorov, and Gode Gravenhorst. 1998. Influence of small-scale structure on radiative transfer and photosynthesis in vegetation canopies. *Journal of Geophysical Research* 103 (1998), 6133–6144.
- Alexander B Kostinski. 2001. On the extinction of radiation by a homogeneous but spatially correlated random medium. *JOSA A* 18, 8 (2001).
- Alexander B Kostinski. 2002. On the extinction of radiation by a homogeneous but spatially correlated random medium: reply to comment. *JOSA A* 19, 12 (2002), 2521–2525.
- Jaroslav Krivánek, Iliyan Georgiev, Toshiya Hachisuka, Petr Vévoda, Martin Šik, Derek Nowrouzezahrai, and Wojciech Jarosz. 2014. Unifying points, beams, and paths in volumetric light transport simulation. *ACM Trans. Graph.* 33, 4 (2014).
- Peter Kutz, Ralf Habel, Yining Karl Li, and Jan Novák. 2017. Spectral and Decomposition Tracking for Rendering Heterogeneous Volumes. *ACM Trans. Graph.* 36, 4 (2017).
- Eric P Lafortune and Yves D Willems. 1996. Rendering participating media with bidirectional path tracing. In *Rendering Techniques '96*.
- Edward W Larsen. 2007. A generalized Boltzmann equation for non-classical particle transport. In *Proceedings of the International Conference on Mathematics and Computations and Supercomputing in Nuclear Applications*.
- Edward W Larsen and Richard Vasques. 2011. A generalized linear Boltzmann equation for non-classical particle transport. *Journal of Quantitative Spectroscopy and Radiative Transfer* 112, 4 (2011).
- Michael L Larsen and Aaron S Clark. 2014. On the link between particle size and deviations from the Beer–Lambert–Bouguer law for direct transmission. *Journal of Quantitative Spectroscopy and Radiative Transfer* 133 (2014), 646–651.
- C D Levermore, G C Pomraning, D L Sanzo, and J Wong. 1986. Linear transport theory in a random medium. *Journal of mathematical physics* 27, 10 (1986).
- Jorge Lopez-Moreno, David Miraut, Gabriel Cirio, and Miguel A. Otaduy. 2015. Sparse GPU Voxelization of Yarn-Level Cloth. *Computer Graphics Forum* 36, 1 (2015).
- Guillaume Loubet and Fabrice Neyret. 2017. Hybrid mesh-volume LoDs for all-scale pre-filtering of complex 3D assets. *Computer Graphics Forum* 36 (2017).
- S Lovejoy, G Brosamlen, and B Watson. 1995. Scattering in multifractal media. In *Particle Transport in Stochastic Media*.

- George Marsaglia and Wai Wan Tsang. 2000. A simple method for generating gamma variables. *ACM Transactions on Mathematical Software (TOMS)* 26, 3 (2000), 363–372.
- Alexander Marshak, Anthony Davis, Warren Wiscombe, and Robert Cahalan. 1998. Radiative effects of sub-mean free path liquid water variability observed in stratiform clouds. *Journal of Geophysical Research: Atmospheres* 103, D16 (1998), 19557–19567.
- Johannes Meng, Marios Papas, Ralf Habel, Carsten Dachsbacher, Steve Marschner, Markus Gross, and Wojciech Jarosz. 2015. Multi-Scale Modeling and Rendering of Granular Materials. *ACM Trans. Graph.* 34, 4 (2015).
- Jonathan T Moon, Bruce Walter, and Stephen R Marschner. 2007. Rendering discrete random media using precomputed scattering solutions. In *Proceedings of EGSR*.
- Thomas Müller, Marios Papas, Markus Gross, Wojciech Jarosz, and Jan Novák. 2016. Efficient Rendering of Heterogeneous Polydisperse Granular Media. *ACM Trans. Graph.* 35, 6 (2016).
- William I Newman, Jeffrey K Lew, George L Siscoe, and Robert G Fovell. 1995. Systematic effects of randomness in radiative transfer. *Journal of the atmospheric sciences* 52, 4 (1995).
- Fabrice Neyret. 1998. Modeling, animating, and rendering complex scenes using volumetric textures. *IEEE Transactions on Visualization and Computer Graphics* 4, 1 (1998), 55–70.
- Jan Novák, Andrew Selle, and Wojciech Jarosz. 2014. Residual Ratio Tracking for Estimating Attenuation in Participating Media. *ACM Trans. Graph.* 33, 6 (2014).
- Jouni I Peltoniemi and Kari Lumme. 1992. Light scattering by closely packed particulate media. *JOSA A* 9, 8 (1992).
- Iman Sadeghi, Adolfo Munoz, Philip Laven, Wojciech Jarosz, Francisco Seron, Diego Gutierrez, and Henrik Wann Jensen. 2012. Physically-based simulation of rainbows. *ACM Trans. Graph.* 31, 1 (2012).
- Kai Schröder, Reinhard Klein, and Arno Zinke. 2011. A Volumetric Approach to Predictive Rendering of Fabrics. *Computer Graphics Forum* 30, 4 (2011).
- Raymond A Shaw, Alexander B Kostinski, and Daniel D Lanterman. 2002. Super-exponential extinction of radiation in a negatively correlated random medium. *Journal of quantitative spectroscopy and radiative transfer* 75, 1 (2002), 13–20.
- László Szirmay-Kalos, Iliyan Georgiev, Milán Magdics, Balázs Molnár, and Dávid Légrády. 2017. Unbiased Estimators to Render Procedurally Generated Inhomogeneous Participating Media. *Computer Graphics Forum* 36, 2 (2017). EUROGRAPHICS 2017.
- Jean Taine, Fabien Bellet, Vincent Leroy, and Estelle Iacona. 2010. Generalized radiative transfer equation for porous medium upscaling: Application to the radiative Fourier law. *International Journal of Heat and Mass Transfer* 53, 19 (2010), 4071–4081.
- Richard Vasques and Edward W Larsen. 2014. Non-classical particle transport with angular-dependent path-length distributions. I: Theory. *Annals of Nuclear Energy* 70 (2014), 292–300.
- Eric Veach. 1997. *Robust Monte Carlo methods for light transport simulation*. Ph.D. Dissertation, Stanford.
- E. Woodcock, T. Murphi, P. Hemmings, and S. Longworth. 1965. Techniques used in the GEM code for Monte Carlo neutronics calculations in reactors and other systems of complex geometry. In *Proc. Conf. Applications of Computing Methods to Reactors, ANL-7050*.
- Magnus Wrenninge, Ryusuke Villemin, and Christophe Hery. 2017. *Path Traced Sub-surface Scattering using Anisotropic Phase Functions and Non-Exponential Free Flights*. Technical Report Pixar Technical Memo 17-07. Pixar Inc.
- Douglas R Wyman, Michael S Patterson, and Brian C Wilson. 1989. Similarity relations for the interaction parameters in radiation transport. *Applied optics* 28, 24 (1989), 5243–5249.
- Shuang Zhao, Wenzel Jakob, Steve Marschner, and Kavita Bala. 2011. Building volumetric appearance models of fabric using micro CT imaging. *ACM Trans. Graph.* 30, 4 (2011).
- Shuang Zhao, Wenzel Jakob, Steve Marschner, and Kavita Bala. 2012. Structure-aware synthesis for predictive woven fabric appearance. *ACM Trans. Graph.* 31, 4 (2012).
- Shuang Zhao, Ravi Ramamoorthi, and Kavita Bala. 2014. High-order similarity relations in radiative transfer. *ACM Transactions on Graphics (TOG)* 33, 4 (2014).
- Shuang Zhao, Lifan Wu, Frédo Durand, and Ravi Ramamoorthi. 2016. Downsampling Scattering Parameters for Rendering Anisotropic Media. *ACM Trans. Graph.* 35, 6 (2016).

S.1 MIXTURES OF SCATTERERS

For media made up of a mixture of scatterers \mathcal{P} , we compute the differential extinction probabilities $\Sigma(\mathbf{x}, t)$ (for both scatterer-to-scatterer and source-to-scatterer transport) as

$$\Sigma(\mathbf{x}, t) = \sum_{k \in \mathcal{P}} w_k \Sigma_k(\mathbf{x}, t), \quad (\text{S.26})$$

where the weights w_k represent the probability of having a scatterer of type $k \in \mathcal{P}$ ($\sum_{k \in \mathcal{P}} w_k = 1$), and $\Sigma_k(\mathbf{x}, t)$ is the differential extinction probability of each type. For the phase function and scattering

albedo, we have

$$\Lambda(\mathbf{x}, t) = \sum_{k \in \mathcal{P}} \frac{w_k \Sigma_k(\mathbf{x}, t)}{\sum_{k \in \mathcal{P}} w_k \Sigma_k(\mathbf{x}, t)} \Lambda_k(\mathbf{x}, t), \quad (\text{S.27})$$

$$f_r(\mathbf{x}, \omega_i, \omega_o, t) = \sum_{k \in \mathcal{P}} \frac{w_k \Sigma_k(\mathbf{x}, t) \Lambda_k(\mathbf{x}, t)}{\sum_{k \in \mathcal{P}} w_k \Sigma_k(\mathbf{x}, t) \Lambda_k(\mathbf{x}, t)} f_{r,k}(\mathbf{x}, \omega_i, \omega_o, t), \quad (\text{S.28})$$

Last, using Equations (S.26) to (S.28), we can compute the scattering operator for a mixture of scatterers as

$$\mathbf{B}(\mathbf{x}, \omega_i, \omega_o, t) = \sum_{k \in \mathcal{P}} w_k \mathbf{B}_k(\mathbf{x}, \omega_i, \omega_o, t). \quad (\text{S.29})$$

S.2 MODELING DIRECTIONAL CORRELATION

Similar to the anisotropy on the cross section described by Jakob et al. [2010], the scatterers correlation might have also an important directional effect, as illustrated in Figure 4 and observed by Vasques and Larsen [2014]. By considering the directional dependency on both $p_C(C)$ and σ , we transform Equation (18) into:

$$\mu p_r(\mu; \omega_o) = C p_C(C; \omega_o) \sigma(\omega_o), \quad (\text{S.30})$$

where $p_C(C; \omega_o)$ and $\bar{\sigma}$ are the probability distribution of the concentration and the mean cross section along ω_o respectively.

To model $p_C(C; \omega_o)$, we noted that its only varying parameter is its variance, which we redefine as a directional function $\text{Var}(C; \omega_o) \in \Omega$. Following the same approach as the SGGX model [Heitz et al. 2015], we model $\text{Var}(C; \omega_o)$ as a zero-mean ellipsoid, using the matrix \mathbf{V} defining the eigenspace of the variance of the projected concentration in Ω (see [Heitz et al. 2015] for details). We thus obtain:

$$\text{Var}(C; \omega_o) = \sqrt{\omega_o^T \mathbf{V} \omega_o}. \quad (\text{S.31})$$

For each direction ω_o , we first obtain the projected variance, and then define the corresponding gamma distribution $\Gamma(C; \alpha(\omega_o), \beta(\omega_o))$ with $\alpha(\omega_o)$ and $\beta(\omega_o)$ computed from \bar{C} and $\text{Var}(C; \omega_o)$. This has several benefits over other directional distributions: it is compact and efficient to evaluate; it supports anisotropy on the main axes; it is symmetric, smooth and non-negative in the full domain Ω ; and it is intuitive to characterize.

S.3 THE GENERALIZED BOLTZMANN EQUATION

Here we include for completeness the derivations of the Generalized Boltzmann Equation (GBE) by Larsen and Vasques [2007; 2011].

Let us define $N(\mathbf{x}, \omega_o, t) dV d\Omega dt$ [$\text{m}^{-3} \text{sr}^{-1} \text{s}^{-1} \text{m}^{-1}$] as the number of particles in $dV d\Omega dt$ over \mathbf{x} and ω_o that have traveled a distance t since its last interaction (scattering or emission). By considering the net flux of particles $\Phi(\mathbf{x}, \omega_o, t)$ as the number of particles moving a distance dt in a differential time dt we get

$$\begin{aligned} \Phi(\mathbf{x}, \omega_o, t) &= \frac{dt}{dt} N(\mathbf{x}, \omega_o, t) \quad [\text{m}^{-2} \text{sr}^{-1} \text{s}^{-1} \text{m}^{-1}] \\ &= v N(\mathbf{x}, \omega_o, t), \end{aligned} \quad (\text{S.32})$$

where $v = \frac{dt}{dt}$ [m s^{-1}] is the speed of the particles.

By using the classic conservation equation that relates the sources of gain and loss of particles with the rate of change of particles, we

get (we use Arvo's notation [1993]):

$$\frac{d}{dt}N(\mathbf{x}, \omega_o, t) = \underbrace{(\mathbf{E}(\mathbf{x}, \omega_o, t) + \mathbf{C}_{\text{in}}(\mathbf{x}, \omega_o, t))}_{\text{gains}} - \underbrace{(\mathbf{S}(\mathbf{x}, \omega_o, t) + \mathbf{C}_{\text{ext}}(\mathbf{x}, \omega_o, t))}_{\text{losses}}, \quad (\text{S.33})$$

with $\mathbf{E}(\mathbf{x}, \omega_o, t)$ and $\mathbf{C}_{\text{in}}(\mathbf{x}, \omega_o, t)$ the gains due to particles emission (source) and inscattering respectively, and $\mathbf{S}(\mathbf{x}, \omega_o, t)$ and $\mathbf{C}_{\text{ext}}(\mathbf{x}, \omega_o, t)$ the losses due to particles leaking (streaming) and extinction due to absorption and outscattering.

In the classic steady-state Boltzmann Equation (and therefore the RTE), it holds that the particles are in equilibrium, and therefore $\frac{d}{dt}N(\mathbf{x}, \omega_o, t) = 0$. However, the introduction on the t dependence on $N(\mathbf{x}, \omega_o, t)$ introduces a non-zero particles rate over $(\mathbf{x}, \omega_o, t)$. By using the relationship in Equation (S.32), we can compute the rate of change in the number of particles in $dV d\Omega dt$ around \mathbf{x}, ω_o, t as

$$\begin{aligned} \frac{d}{dt}N(\mathbf{x}, \omega_o, t)dV d\Omega dt &= \frac{d}{v dt}v N(\mathbf{x}, \omega_o, t)dV d\Omega dt \\ &= \frac{d}{dt}\Phi(\mathbf{x}, \omega_o, t)dV d\Omega dt. \end{aligned} \quad (\text{S.34})$$

Using a similar relationship, we can compute net rate of particles leaking out of dV around \mathbf{x} in direction ω_o after traveling a distance t as

$$\mathbf{S}(\mathbf{x}, \omega_o, t) = \omega_o \cdot \nabla \Phi(\mathbf{x}, \omega_o, t)dV d\Omega dt. \quad (\text{S.35})$$

Now, let us define $\Sigma(t)$ [m^{-1}] as the differential probability of extinction, and $\Sigma(t)dt$ as the probability of a particle to interact at distance dt after having traveled a distance t since its last interaction (emission or scattering). With these definitions, we can compute the rate of collision (extinction) as

$$\begin{aligned} \mathbf{C}_{\text{ext}}(\mathbf{x}, \omega_o, t) &= \frac{1}{dt}\Sigma(t)dt N(\mathbf{x}, \omega_o, t)dV d\Omega dt \\ &= \frac{dt}{dt}\Sigma(t) N(\mathbf{x}, \omega_o, t)dV d\Omega dt \\ &= \Sigma(t)\Phi(\mathbf{x}, \omega_o, t)dV d\Omega dt. \end{aligned} \quad (\text{S.36})$$

The treatment of inscattering and source terms is slightly more complex, given that they set the *memory* of the particles to $t = 0$. Assuming that scattering and absorbers have the same distribution, and therefore we can formulate the differential probability of scattering as $\Sigma_s(t) = \Lambda \Sigma(t)$ [m^{-1}], with Λ [unitless] the probability of scattering of a particle that has suffered collision (scattering albedo). From Equation (S.36), we can compute the rate of particles colliding at \mathbf{x} from direction ω_i as

$$\begin{aligned} \mathbf{C}_{\text{ext}}(\mathbf{x}, \omega_i) &= \int_0^\infty \mathbf{C}_{\text{ext}}(\mathbf{x}, \omega_i, t)dt \\ &= \left[\int_0^\infty \Sigma(t)\Phi(\mathbf{x}, \omega_i, t)dt \right] dV d\Omega. \end{aligned} \quad (\text{S.37})$$

Then, by multiplying $\mathbf{C}_{\text{ext}}(\mathbf{x}, \omega_i)$ by the phase function $f_r(\omega_i, \omega_o)$ [sr^{-1}] and the scattering albedo Λ , and integrating over the sphere Ω we get

$$\left[\Lambda \int_\Omega f_r(\omega_i, \omega_o)\mathbf{C}_{\text{ext}}(\mathbf{x}, \omega_i)d\omega_i \right] dV d\Omega. \quad (\text{S.38})$$

Since as particles emerge from a scattering event they reset their value t to $t = 0$, then the path length spectrum of inscattering is a delta function $\delta(t)$. Multiplying Equation (S.38) by $\delta(t)dt$ we get $\mathbf{C}_{\text{in}}(\mathbf{x}, \omega_o, t)$ as

$$\mathbf{C}_{\text{in}}(\mathbf{x}, \omega_o, t) = \delta(t)\Lambda \left[\int_\Omega f_r(\omega_i, \omega_o)\mathbf{C}_{\text{ext}}(\mathbf{x}, \omega_i)d\omega_i \right] dV d\Omega dt. \quad (\text{S.39})$$

Similarly to scattering, emission also requires to set particles to $t = 0$. Following the same reasoning as before, we define the source term $\mathbf{E}(\mathbf{x}, \omega_o, t)$ as:

$$\mathbf{E}(\mathbf{x}, \omega_o, t) = \delta(t)q(\mathbf{x}, \omega_o)dV d\Omega dt, \quad (\text{S.40})$$

where $q(\mathbf{x}, \omega_o)dV d\Omega$ [$\text{m}^{-3} \text{sr}^{-1} \text{s}^{-1}$] is the rate at which particles are emitted by an internal source in \mathbf{x} in direction ω_o .

Substituting Equations (S.35), (S.36), (S.39), and (S.40) into Equation (S.33), and dividing both sides of the equation by $dV d\Omega dt$ we get the final GBE for generic particles transport proposed by Larsen and Vasques [2011, Eq. (2.3)]

$$\begin{aligned} \frac{d}{dt}\Phi(\mathbf{x}, \omega_o, t) + \omega_o \cdot \nabla \Phi(\mathbf{x}, \omega_o, t) + \Sigma(t)\Phi(\mathbf{x}, \omega_o, t) &= \\ \delta(t)\Lambda \int_0^\infty \Sigma(s) \int_\Omega \Phi(\mathbf{x}, \omega_i, s)f_r(\omega_i, \omega_o)d\omega_i ds + \delta(t)q(\mathbf{x}, \omega_o), \end{aligned} \quad (\text{S.41})$$

Equation (S.41) defines models transport for general particles as a function of their flux $\Phi(\mathbf{x}, \omega_o, t)$. Since we are interested on light, we want to express such equation in terms of radiance. We can then set $v = c$, with c the speed of light, and assuming monoenergetic photons with wavelength λ [Hz^{-1}], then we define the radiance at \mathbf{x} from direction ω_o , that has traveled a distance t since its last interaction as

$$L(\mathbf{x}, \omega_o, t) = \frac{hc}{\lambda} N(\mathbf{x}, \omega_o, t) = \frac{h}{\lambda} \Phi(\mathbf{x}, \omega_o, t), \quad \left[\frac{\text{W}}{\text{m}^2 \text{sr m}} \right] \quad (\text{S.42})$$

with h is Planck's constant. Note that the t -resolved radiance $L(\mathbf{x}, \omega_o, t)$ relates with the classic radiance as:

$$L(\mathbf{x}, \omega_o) = \int_0^\infty L(\mathbf{x}, \omega_o, t)dt. \quad \left[\frac{\text{W}}{\text{m}^2 \text{sr}} \right] \quad (\text{S.43})$$

Similarly, the source term for light $Q(\mathbf{x}, \omega_o)$ is defined in terms of radiant power, and related with $q(\mathbf{x}, \omega_o)$ as

$$Q(\mathbf{x}, \omega_o) = \frac{h}{\lambda} q(\mathbf{x}, \omega_o). \quad \left[\frac{\text{W}}{\text{m}^3 \text{sr}} \right] \quad (\text{S.44})$$

Therefore, by multiplying Equation (S.41) by $h\lambda^{-1}$ we get the GBE in terms of radiance as

$$\begin{aligned} \frac{d}{dt}L(\mathbf{x}, \omega_o, t) + \omega_o \cdot \nabla L(\mathbf{x}, \omega_o, t) + \Sigma(t)L(\mathbf{x}, \omega_o, t) &= \\ \delta(t)\Lambda \int_0^\infty \Sigma(s) \int_\Omega L(\mathbf{x}, \omega_i, s)f_r(\omega_i, \omega_o)d\omega_i ds + \delta(t)Q(\mathbf{x}, \omega_o). \end{aligned} \quad (\text{S.45})$$

Finally, we can obtain the equivalent delta-less form presented in Equation (5): We first set Equation (S.45) for $t > 0$ as

$$\frac{d}{dt}L(\mathbf{x}, \omega_o, t) + \omega_o \cdot \nabla L(\mathbf{x}, \omega_o, t) + \Sigma(t)L(\mathbf{x}, \omega_o, t) = 0. \quad (\text{S.46})$$

Then, to define the initial value for $t = 0$ of the ODE defined by Equation (S.46) we operate Equation (S.45) with $\lim_{\epsilon \rightarrow 0} \int_{-\epsilon}^{\epsilon} (\cdot) dt$, and using $L(\mathbf{x}, \omega_o, t) = 0$ for $t < 0$ we define

$$L(\mathbf{x}, \omega_o, 0) = \lim_{t \rightarrow 0^+} L(\mathbf{x}, \omega_o, t) = L(\mathbf{x}, \omega_o, 0^+) \quad (\text{S.47})$$

to obtain

$$L(\mathbf{x}, \omega_o, 0) = \int_0^\infty \Sigma_s(t) \int_\Omega L(\mathbf{x}, \omega_i, t) f_r(\omega_i, \omega_o) d\omega_i dt + Q(\mathbf{x}, \omega_o), \quad (\text{S.48})$$

which is the second line in Equation (5).

S.4 THE RTE AS A SPECIAL CASE OF THE GBE

Here we will see that the classic RTE is a special case of Larsen's Generalized Boltzmann Equation (GBE) [Larsen 2007; Larsen and Vasques 2011], in which the differential extinction probability $\Sigma(t)$ is independent of t , and therefore a constant defined by the extinction coefficient $\Sigma(t) = \mu$.

Let us use the equivalent delta-based form of Equation (5) shown in Equation (S.45). In the classic RTE, the differential probability of extinction is a constant $\Sigma(t) = \mu$, so that Equation (S.45) becomes

$$\begin{aligned} \frac{d}{dt} L(\mathbf{x}, \omega_o, t) + \omega_o \cdot \nabla L(\mathbf{x}, \omega_o, t) + \mu L(\mathbf{x}, \omega_o, t) = \\ \delta(t) \mu_s \int_0^\infty \int_\Omega L(\mathbf{x}, \omega_i, s) f_r(\omega_i, \omega_o) d\omega_i ds + \delta(t) Q(\mathbf{x}, \omega_o) = \\ \delta(t) \mu_s \int_\Omega L(\mathbf{x}, \omega_i) f_r(\omega_i, \omega_o) d\omega_i + \delta(t) Q(\mathbf{x}, \omega_o), \end{aligned} \quad (\text{S.49})$$

where $\mu_s = \Lambda \mu$, $L(\mathbf{x}, \omega_i) = \int_0^\infty L(\mathbf{x}, \omega_i, s) ds$. Then, by operating Equation (S.49) by $\int_{-\epsilon}^\infty (\cdot) dt$ (with $\epsilon \approx 0$; note that we cannot use $\epsilon = 0$ because otherwise the integral of the delta function $\delta(t)$ would be undefined) we get

$$\begin{aligned} L(\mathbf{x}, \omega_o, -\epsilon) + L(\mathbf{x}, \omega_i, \infty) + \omega_o \cdot \nabla L(\mathbf{x}, \omega_o) + \mu L(\mathbf{x}, \omega_o) = \\ \mu_s \int_\Omega L(\mathbf{x}, \omega_i) f_r(\omega_i, \omega_o) d\omega_i + Q(\mathbf{x}, \omega_o). \end{aligned} \quad (\text{S.50})$$

Finally, by using $L(\mathbf{x}, \omega_i, -\epsilon) = L(\mathbf{x}, \omega_i, \infty) = 0$ we get

$$\begin{aligned} \omega_o \cdot \nabla L(\mathbf{x}, \omega_o) + \mu L(\mathbf{x}, \omega_o) = \\ \mu_s \int_\Omega L(\mathbf{x}, \omega_i) f_r(\omega_i, \omega_o) d\omega_i + Q(\mathbf{x}, \omega_o), \end{aligned} \quad (\text{S.51})$$

which is the RTE [Equation (1)].

S.5 FROM OUR EXTENDED GBE TO LARSEN'S GBE

Here we demonstrate that our Extended GBE Section 4 is a generalization of Larsen's GBE [Equation (5)], and how the latter can be obtained from ours.

Our Extended GBE is defined as

$$\begin{aligned} \frac{d}{dt} L(\mathbf{x}, \omega_o, t) + \omega_o \cdot \nabla L(\mathbf{x}, \omega_o, t) + \Sigma_S(\mathbf{x}, t) L_S(\mathbf{x}, \omega_o, t) \\ + \sum_j \Sigma_{Q_j}(\mathbf{x}, t) L_{Q_j}(\mathbf{x}, \omega_o, t) = 0, \end{aligned} \quad (\text{S.52})$$

$$\begin{aligned} L_S(\mathbf{x}, \omega_o, 0) = \int_0^\infty \int_\Omega \left(B_S(\mathbf{x}, \omega_i, \omega_o, t) L_S(\mathbf{x}, \omega_i, t) \right. \\ \left. + \sum_j B_{Q_j}(\mathbf{x}, \omega_i, \omega_o, t) L_{Q_j}(\mathbf{x}, \omega_i, t) \right) d\omega_i dt, \end{aligned} \quad (\text{S.53})$$

$$L_{Q_j}(\mathbf{x}, \omega_o, 0) = Q_j(\mathbf{x}, \omega_o), \quad (\text{S.54})$$

where

$$L(\mathbf{x}, \omega_o, t) = L_S(\mathbf{x}, \omega_o, t) + \sum_j L_{Q_j}(\mathbf{x}, \omega_o, t), \quad (\text{S.55})$$

the differential extinction probabilities for the scattered photons and the (unscattered) photons emitted by light source Q_j are respectively $\Sigma_S(\mathbf{x}, t)$ and $\Sigma_{Q_j}(\mathbf{x}, t)$, the scattering operator for scattered photons is $B_S(\mathbf{x}, \omega_i, \omega_o, t) = \Lambda_S(\mathbf{x}, t) \Sigma_S(\mathbf{x}, t) f_{r,S}(\mathbf{x}, \omega_i, \omega_o, t)$, and $B_{Q_j}(\mathbf{x}, \omega_i, \omega_o, t)$ is the scattering operator for photons emitted by light source Q_j .

Equation (S.52) does not impose any assumption on the correlation between scatterers and sources. If they were somehow positively correlated, so that the scatterers and emitters would have the exact same correlation with respect to extinguishing particles (which could be scatterers or not), then

$$\forall j, \quad \Sigma_S(\mathbf{x}, t) = \Sigma_{Q_j}(\mathbf{x}, t) = \Sigma(\mathbf{x}, t)$$

and

$$\forall j, \quad B_S(\mathbf{x}, \omega_i, \omega_o, t) = B_{Q_j}(\mathbf{x}, \omega_i, \omega_o, t) = B(\mathbf{x}, \omega_i, \omega_o, t).$$

This allows us to transform Equation (S.52) into

$$\begin{aligned} \frac{d}{dt} L(\mathbf{x}, \omega_o, t) + \omega_o \cdot \nabla L(\mathbf{x}, \omega_o, t) \\ + \Sigma(\mathbf{x}, t) \left(L_S(\mathbf{x}, \omega_o, t) + \sum_j L_{Q_j}(\mathbf{x}, \omega_o, t) \right) = \\ \frac{d}{dt} L(\mathbf{x}, \omega_o, t) + \omega_o \cdot \nabla L(\mathbf{x}, \omega_o, t) + \Sigma(\mathbf{x}, t) L(\mathbf{x}, \omega_o, t) = 0, \end{aligned} \quad (\text{S.56})$$

while Equations (S.53) and (S.54) become

$$\begin{aligned} L_S(\mathbf{x}, \omega_o, 0) = \int_0^\infty \int_\Omega B(\mathbf{x}, \omega_i, \omega_o, t) \left(L_S(\mathbf{x}, \omega_i, t) \right. \\ \left. + \sum_j L_{Q_j}(\mathbf{x}, \omega_i, t) \right) d\omega_i dt \end{aligned} \quad (\text{S.57})$$

$$= \int_0^\infty \int_\Omega B(\mathbf{x}, \omega_i, \omega_o, t) L(\mathbf{x}, \omega_o, t) d\omega_i dt,$$

$$L_{Q_j}(\mathbf{x}, \omega_o, 0) = Q_j(\mathbf{x}, \omega_o). \quad (\text{S.58})$$

From Equations (S.55), (S.57), and (S.58) we can simplify the initial value of Equation (S.56) as:

$$L(\mathbf{x}, \omega_o, 0) = \int_0^\infty \int_\Omega L(\mathbf{x}, \omega_i, t) B(\mathbf{x}, \omega_i, \omega_o, t) d\omega_i dt + Q(\mathbf{x}, \omega_o). \quad (\text{S.59})$$

Finally, by removing the spatial dependence on $\Sigma(t)$ and the t -dependence on albedo and phase function from Equations (S.56) and (S.59) we get Larsen's GBE [Equation (5)].

S.6 INTEGRAL FORM OF THE EXTENDED GBE

In this section we compute the integro-differential form of our Extended GBE, modeled in differential form in Equations (S.52) to (S.54). Let us first expand Equation (S.52) by using Equation (S.55) as

$$\begin{aligned} & \frac{d}{dt} L_S(\mathbf{x}, \omega_o, t) + \omega_o \cdot \nabla L_S(\mathbf{x}, \omega_o, t) + \Sigma_S(\mathbf{x}, t) L_S(\mathbf{x}, \omega_o, t) \\ & + \sum_j \left(\frac{d}{dt} L_{Q_j}(\mathbf{x}, \omega_o, t) + \omega_o \cdot \nabla L_{Q_j}(\mathbf{x}, \omega_o, t) + \Sigma_{Q_j}(\mathbf{x}, t) L_{Q_j}(\mathbf{x}, \omega_o, t) \right) \\ & = 0. \end{aligned} \quad (\text{S.60})$$

This expression is a sum of multiple independent differential equations on $L_S(\mathbf{x}, \omega_o, t)$ and $L_{Q_j}(\mathbf{x}, \omega_o, t)$ with $j \in [1, \infty)$. Since they are independent on each other, we can solve them individually, and then put them back together. Let us first start with the simpler case of L_{Q_j} , by setting $L_S(\mathbf{x}, \omega_o, t) = 0$ and $L_{Q_k} = 0$ for all $k \neq j$, and getting

$$\begin{aligned} & \frac{d}{dt} L_{Q_j}(\mathbf{x}, \omega_o, t) + \omega_o \cdot \nabla L_{Q_j}(\mathbf{x}, \omega_o, t) + \Sigma_{Q_j}(\mathbf{x}, t) L_{Q_j}(\mathbf{x}, \omega_o, t) = 0, \\ & L_{Q_j}(\mathbf{x}, \omega_o, 0) = Q_j(\mathbf{x}, \omega_o). \end{aligned} \quad (\text{S.61})$$

By solving this partial differential equation we get

$$\begin{aligned} L_{Q_j}(\mathbf{x}, \omega_o, t) &= L_{Q_j}(\mathbf{x}_t, \omega_o, 0) e^{-\int_0^t \Sigma_{Q_j}(\mathbf{x}, s) ds} \\ &= Q_j(\mathbf{x}, \omega_o) T_{Q_j}(\mathbf{x}, \mathbf{x}_t), \end{aligned} \quad (\text{S.62})$$

where $\mathbf{x}_t = \mathbf{x} - \omega_o t$ and $T_{Q_j}(\mathbf{x}, \mathbf{x}_t) = e^{-\int_0^t \Sigma_{Q_j}(\mathbf{x}, s) ds}$. Then we apply the definite integral on t in the interval $[0, \infty)$ to remove the t dependence as

$$\begin{aligned} L_{Q_j}(\mathbf{x}, \omega_o) &= \int_0^\infty L_{Q_j}(\mathbf{x}, \omega_o, t) dt \\ &= \int_0^\infty Q_j(\mathbf{x}, \omega_o) T_{Q_j}(\mathbf{x}, \mathbf{x}_t) dt. \end{aligned} \quad (\text{S.63})$$

Now let's consider the case of $L_S(\mathbf{x}, \omega_o, t)$ by setting $L_{Q_k} = 0$ for all k

$$\begin{aligned} & \frac{d}{dt} L_S(\mathbf{x}, \omega_o, t) + \omega_o \cdot \nabla L_S(\mathbf{x}, \omega_o, t) + \Sigma_S(\mathbf{x}, t) L_S(\mathbf{x}, \omega_o, t) = 0, \\ & L_S(\mathbf{x}, \omega_o, 0) = \int_0^\infty \int_\Omega \left(B_S(\mathbf{x}, \omega_i, \omega_o, t) L_S(\mathbf{x}, \omega_i, t) \right. \\ & \quad \left. + \sum_j B_{Q_j}(\mathbf{x}, \omega_i, \omega_o, t) L_{Q_j}(\mathbf{x}, \omega_i, t) \right) d\omega_i dt. \end{aligned} \quad (\text{S.64})$$

Again, by solving Equation (S.64), and applying $L_S(\mathbf{x}, \omega_o, 0) = S(\mathbf{x}, \omega_o)$ we get

$$\begin{aligned} L_S(\mathbf{x}, \omega_o, t) &= L_S(\mathbf{x}, \omega_o, 0) e^{-\int_0^t \Sigma_S(\mathbf{x}, s) ds} \\ &= S(\mathbf{x}, \omega_o) T_{L_S}(\mathbf{x}, \mathbf{x}_t). \end{aligned} \quad (\text{S.65})$$

which by applying again $\int_0^\infty (\cdot) dt$ gives

$$\begin{aligned} L_S(\mathbf{x}, \omega_o) &= \int_0^\infty L_S(\mathbf{x}, \omega_o, t) dt \\ &= \int_0^\infty S(\mathbf{x}, \omega_o) T_{L_S}(\mathbf{x}, \mathbf{x}_t) dt. \end{aligned} \quad (\text{S.66})$$

Finally, from Equations (S.63) and (S.66) we compute the total radiance $L(\mathbf{x}, \omega_o)$ via Equation (S.55) as

$$\begin{aligned} L(\mathbf{x}, \omega_o) &= \int_0^\infty T_S(\mathbf{x}, \mathbf{x}_t) S(\mathbf{x}_t, \omega_o) \\ & \quad + \sum_j T_{Q_j}(\mathbf{x}, \mathbf{x}_t) Q_j(\mathbf{x}_t, \omega_o) dt. \end{aligned} \quad (\text{S.67})$$

S.7 SIMPLIFYING EQUATION (15)

In this section we include the derivations taking from Equation (15) to Equation (16) in Section 5.1 of the main text. Equation (15) computes the transmittance of an incoming beam as

$$T(t) = \int_0^\infty \int_0^\infty p_L(L_i) p_\tau(\mu; L_i) \frac{L_i}{\hat{L}_i} \mathcal{T}(\mu t) d\mu dL_i. \quad (\text{S.68})$$

where $p_L(L_i)$ is a probability distribution describing the incoming radiance L_i , $p_\tau(\mu; L_i)$ is the conditional probability distribution describing the distribution of particles as a function of the incoming radiance L_i , and $\hat{L}_i = \int_0^\infty p_L(L_i) L_i dL_i$ is the total incoming radiance.

The first assumption we make is that the spatial distributions of incoming light and scatterers are decorrelated. This means that $p_L(L_i)$ and $p_\tau(\mu)$ are independent, so that $p_\tau(\mu; L_i) = p_\tau(\mu)$. This transforms Equation (S.68) into

$$\begin{aligned} T(t) &= \int_0^\infty \int_0^\infty p_L(L_i) p_\tau(\mu) \frac{L_i}{\hat{L}_i} \mathcal{T}(\mu t) d\mu dL_i \\ &= \int_0^\infty p_\tau(\mu) \mathcal{T}(\mu t) \int_0^\infty p_L(L_i) \frac{L_i}{\hat{L}_i} dL_i d\mu \\ &= \int_0^\infty p_\tau(\mu) \mathcal{T}(\mu t) \frac{\hat{L}_i}{\hat{L}_i} d\mu \\ &= \int_0^\infty p_\tau(\mu) \mathcal{T}(\mu t) d\mu. \end{aligned} \quad (\text{S.69})$$

Finally, $\mathcal{T}(\mu t)$ is the attenuation function, that describes the probability of extinction of an *individual ray*. Note that we have used a generic attenuation function $\mathcal{T}(\tau_t(\mathbf{r}))$; if the particles distribution is random (although correlated) then the extinction at each differential ray of the beam is Poissonian, holding $\mathcal{T}(\tau_t(\mathbf{r})) = e^{-\mu t}$. In other cases, in particular in ordered media presenting negative correlation, this attenuation does not hold and extinction becomes a Bernoulli stochastic process, which in the limit reduces to a deterministic linear attenuation. By keeping the exponential attenuation, we transform Equation (S.68) into

$$T(t) = \int_0^\infty p_\tau(\mu) e^{-\mu t} d\mu. \quad (\text{S.70})$$

S.8 THE RTE AS A SPECIAL CASE OF OUR LOCAL MODEL

In this section we show how the exponential transmittance predicted by the Beer-Lambert law is a particular case of our model in Section 5.1, in particular how Equation (15), its simplified form [Equation (16)], and the final gamma-based transmittance [Equation (20)] converge to $T(t) = e^{-\bar{\mu} t}$, with $\bar{\mu}$ the mean extinction in the differential volume dV .

S.8.1 Equation (15) to exponential transmittance

Starting from Equation (S.68) [Equation (15) in the paper], let us first define the scatterers distribution by setting the probability distribution of extinction $p_\tau(\mu)$. In the classic RTE the assumption is that particles are uniformly distributed in a differential volume, so that the extinction probability is always the same $\bar{\mu}$. Mathematically, this is equivalent to setting

$$p_\tau(\mu) = \delta(\bar{\mu} - \mu), \quad (\text{S.71})$$

where $\delta(s)$ is the Dirac delta function. With that, we can transform Equation (S.68) into

$$\begin{aligned} T(t) &= \int_0^\infty \int_0^\infty p_L(L_i) \delta(\bar{\mu} - \mu) \frac{L_i}{\hat{L}_i} \mathcal{T}(\mu t) d\mu dL_i \\ &= \int_0^\infty p_L(L_i) \frac{L_i}{\hat{L}_i} \int_0^\infty \delta(\bar{\mu} - \mu) \mathcal{T}(\mu t) d\mu dL_i \\ &= \int_0^\infty \frac{L_i}{\hat{L}_i} dL_i \mathcal{T}(\bar{\mu} t) \\ &= \frac{\hat{L}_i}{\hat{L}_i} \mathcal{T}(\bar{\mu} t) \\ &= \mathcal{T}(\bar{\mu} t). \end{aligned} \quad (\text{S.72})$$

Finally, we need to define the attenuation process of extinction defined by $\mathcal{T}(\mu t)$. Since we are assuming that particles are randomly distributed, then we can safely assume that $\mathcal{T}(\mu t)$ is a Poissonian process (see Section S.7), where $\mathcal{T}(\mu t) = e^{-\mu t}$ holds. By substitution, we therefore transform Equation (S.72) into the exponential transmittance $T(t) = e^{-\bar{\mu} t}$. Finally, by applying that $\Sigma(t) = p(t)/T(t)$ we can verify that

$$\Sigma(t) = \frac{p(t)}{T(t)} = \left| \frac{dT(t)}{dt} \right| \frac{1}{T(t)} = \frac{\bar{\mu} e^{-\bar{\mu} t}}{e^{-\bar{\mu} t}} = \bar{\mu}, \quad (\text{S.73})$$

which is the t -independent classic form of the differential extinction probability, and which as shown in Section S.4 reduces the GBE to the classic RTE.

S.8.2 Equation (16) to exponential transmittance

Following the same procedure as in the previous section it is easy to verify that by defining a uniform distribution of particles with mean extinction $\bar{\mu}$ via Equation (S.71) we reduce Equation (16) to the exponential decay as:

$$\begin{aligned} T(t) &= \int_0^\infty p_\tau(\mu) e^{-\mu t} d\mu \\ &= \int_0^\infty \delta(\bar{\mu} - \mu) e^{-\mu t} d\mu \\ &= e^{-\bar{\mu} t}. \end{aligned} \quad (\text{S.74})$$

S.8.3 Equation (20) to exponential transmittance

Finally, we will show that practical gamma-based form of transmittance [Equation (20)], defined as

$$\begin{aligned} T(t) &= \int_0^\infty \Gamma(C; \alpha, \beta) e^{-\mu^\sigma t} d\mu \\ &= \left(1 + \frac{\bar{\sigma} \cdot t}{\beta} \right)^{-\alpha}, \end{aligned} \quad (\text{S.75})$$

with $\Gamma(C; \alpha, \beta)$ the gamma distribution, $\alpha = \bar{C}^2 \cdot \text{Var}(C)^{-1}$, $\beta = \bar{C} \cdot \text{Var}(C)^{-1}$, with \bar{C} and $\text{Var}(C)$ the mean and variance of particles concentration C respectively, and σ the mean cross section. By plugging the definition of α and β in Equation (S.75) we get

$$T(t) = \left(1 + \sigma t \frac{\text{Var}(C)}{\bar{C}} \right)^{-\frac{\bar{C}^2}{\text{Var}(C)}}. \quad (\text{S.76})$$

Then, by applying the limit to Equation (S.77) we get

$$\lim_{\text{Var}(C) \rightarrow 0} \left(1 + \sigma t \frac{\text{Var}(C)}{\bar{C}} \right)^{-\frac{\bar{C}^2}{\text{Var}(C)}} = e^{-\bar{C} \sigma t}. \quad (\text{S.77})$$

Finally, by using $\bar{\mu} = \bar{C} \sigma$ we get $T(t) = e^{-\bar{\mu} t}$. A complementary way of formulating this proof is by noticing that $\lim_{\text{Var}(C) \rightarrow 0} \Gamma(C; \alpha, \beta) = \delta(\bar{C} - C)$, which results into a very similar derivation to Section S.8.2.

S.9 DERIVATION OF SAMPLING PROCEDURES FOR EQUATION (20)

In Section 5.2 of the main text we define transmittance for distance t in correlated media as [Equation (20)]

$$T(t) = \left(1 + \frac{\bar{\sigma} \cdot t}{\beta} \right)^{-\alpha}, \quad (\text{S.78})$$

with $\alpha = \bar{C}^2 \cdot \text{Var}(C)^{-1}$, $\beta = \bar{C} \cdot \text{Var}(C)^{-1}$, with \bar{C} and $\text{Var}(C)$ the mean and variance of particles concentration C respectively, and σ the mean cross section.

General case $\alpha \in (0, \infty)$

In order to sample a distance t with respect to Equation (20) we need to define the probability function of sampling distance t as $p(t)$. We can compute it using the physical definition of transmittance as:

$$T(t) = \int_t^\infty p(t') dt', \quad (\text{S.79})$$

from which follows [Equation (21)]

$$\begin{aligned} p(t) &= \left| \frac{dT(t)}{dt} \right| \\ &= \alpha \sigma \frac{\left(\frac{\sigma t}{\beta} + 1 \right)^{-(1+\alpha)}}{\beta}, \end{aligned} \quad (\text{S.80})$$

which has as CDF

$$P(t) = T(0) - T(t) = 1 - T(t). \quad (\text{S.81})$$

We sample $T(t)$ by using the inverse of Equation (S.81) as

$$t(\xi) = -\frac{\beta}{\sigma} \left(1 - \sqrt[\alpha]{1 - \xi} \right). \quad (\text{S.82})$$

Sampling Equation (20) for $\alpha \in (0, 1)$ Unfortunately, Equation (S.80) is not proportional to Equation (S.79), which is desirable for minimizing variance in Monte Carlo integration. In order to compute such sampling probability we impose $p(t) \propto T(t)$ as $p(t) = C T(t)$, where C is a constant that ensures that $\int_0^\infty p(t') dt' = 1$. We can thus write

$$C = \frac{1}{\int_0^\infty T(t') dt'}. \quad (\text{S.83})$$

Solving the integral in the denominator we get

$$\int_0^\infty \left(1 + \frac{\sigma \cdot t'}{\beta}\right)^{-\alpha} dt' = \frac{(\beta + \sigma t')}{\sigma(1-\alpha)} \left(1 + \frac{\sigma \cdot t'}{\beta}\right)^{-\alpha} \Big|_0^\infty \quad (\text{S.84})$$

$$= -\frac{\beta}{\sigma(1-\alpha)} + \lim_{t' \rightarrow \infty} \frac{(\beta + \sigma t')}{\sigma(1-\alpha)} \left(1 + \frac{\sigma \cdot t'}{\beta}\right)^{-\alpha},$$

which is convergent for $\alpha > 1$ to

$$\int_0^\infty T(t') dt' = -\frac{\beta}{\sigma(1-\alpha)} \quad (\text{S.85})$$

Finally, by using Equations (S.83) and (S.85) we can compute the sampling probability as [Equation (23)]

$$p(t) = -\sigma \frac{1-\alpha}{\beta} \left(1 + \frac{\sigma}{\beta} t\right)^{-\alpha} = -\sigma \frac{1-\alpha}{\beta} T(t), \quad (\text{S.86})$$

which has CDF

$$P(t) = 1 - \left(1 + \frac{\sigma}{\beta} t\right)^{1-\alpha}. \quad (\text{S.87})$$

Finally, we sample Equation (S.86) by inverting Equation (S.87) as [Equation (24)]

$$t(\xi) = P(t)^{-1} = -\frac{\beta}{\sigma} \left(1 - \sqrt[1-\alpha]{1-\xi}\right). \quad (\text{S.88})$$

S.10 ADDITIONAL PROBABILITY DISTRIBUTIONS OF EXTINCTION

Here we list additional probability distributions of extinction $p(t)$ used in the results of the paper. The first one (Section S.10.1) a perfect negative correlation results into a Bernoulli process (rather than a Poisson process), leading to linear transmittance; the second one (Section S.10.2) models $p(t)$ as a gamma probability distribution. Note that the later is different from our local model in Section 5.2. This second $p(t)$ is important, given that a gamma distribution is in general in good agreement with measured (or computed via Monte Carlo simulations) probability distributions of extinction in particulate materials (see e.g. [Meng et al. 2015, Figure 6]). In the following we list the close-forms of transmittance $T(t)$, probability distribution of extinction $p(t)$, and differential probability of extinction $\Sigma(t)$.

S.10.1 Perfect negative correlation

We define this probability distribution of extinction via the mean extinction coefficient $\bar{\mu}$, as

$$T(t) = \max(0, 1 - \bar{\mu} t), \quad (\text{S.89})$$

$$p(t) = \begin{cases} \mu & \text{for } t < \frac{1}{\mu} \\ 0 & \text{elsewhere} \end{cases} \quad (\text{S.90})$$

$$\Sigma(t) = \begin{cases} \frac{\mu}{1-\bar{\mu}t} & \text{for } t < \frac{1}{\mu} \\ 0 & \text{elsewhere} \end{cases}. \quad (\text{S.91})$$

We can sample Equation (S.90) by using

$$t(\xi) = \frac{\xi}{\mu}, \quad (\text{S.92})$$

with $\xi \in (0, 1)$ a uniform random number.

S.10.2 Gamma probability distribution of extinction

In this case, the gamma distribution defines the probability distribution of extinction $p(t) = \Gamma(t; k, \theta)$, parametrized by the parameters $k = \bar{t}^2/\text{Var}(t)$ and $\theta = \text{Var}(t)/\bar{t}$, where \bar{t} is the mean free path, and $\text{Var}(t)$ the variance of the distribution. Note that to avoid confusion with Equation (19) used as $p_C(C)$, we used the alternative parametrization of the gamma distribution, where $k = \alpha$ and $\theta = \beta^{-1}$. This distribution leads to

$$T(t) = 1 - \frac{\gamma_p(k, \theta^{-1} t)}{\gamma(k)}, \quad (\text{S.93})$$

$$p(t) = \Gamma(t; k, \theta), \quad (\text{S.94})$$

$$\Sigma(t) = \frac{\Gamma(t; k, \theta)}{1 - \frac{\gamma_p(k, \theta^{-1} t)}{\gamma(k)}}, \quad (\text{S.95})$$

where $\gamma_p(s, x) = \int_0^x t^{s-1} e^{-t} dt$ is the incomplete gamma function, and $\gamma(x)$ is the gamma function. In order to sample Equation (S.94) we do not have a closed form, and need to use numerical methods. In our case, we used the rejection method by Marsaglia and Tsang [2000], which can sample the full space of k , and with cost approximately constant with k .

S.11 DETAILS ON FIGURE 2

In order to validate the existence of non-exponential transmittance, in addition to findings from other fields such as neutron transport or atmospheric sciences, we performed a simple experiment where we capture the transmittance of different correlated (non-exponential) and uncorrelated (exponential) media. For capture, we use a setup inspired in Meng et al. [Meng et al. 2015, Figure 3], where we filled a glass-made vase with the material. The vase was placed on top of a mobile flash for lighting, and captured using a Nikon D200 placed over the vase.

We capture a set of HDR images of increasing thickness for each material. Each image was captured by multi-bracketing 36 RAW images, with fixed aperture set at 4.9, ISO-1600, and exposition time ranging from 1/6400 s to 1/2 s. To get rid of the effect of the container we also captured an HDR image of the empty glass.

Finally, to assess whether the exponential transmittance holds or not on the captured materials, we fit them to an exponential function. As shown in Figure 2, for correlated materials this fitness is not very accurate, while diluted milk shows a very good fit, as expected.

S.12 RENDERING CONVERGENCE

In order to evaluate whether our new model increases variance, we evaluate the convergence of our model with respect to classic exponential transport. We perform this evaluation in the scenes shown in Figures 1 and 17, for three different types of media: classic exponential, and non-exponential with positive and negative correlation. We used volumetric path tracing for rendering. Figure S.19 shows how the error of both media converge in a similar rate with the number of samples (as expected), but that the increment in variance is marginal, and in fact only observable in the case of positive correlation, where the increased transmittance might result in an increase of variance. A similar behavior is observed with the converge

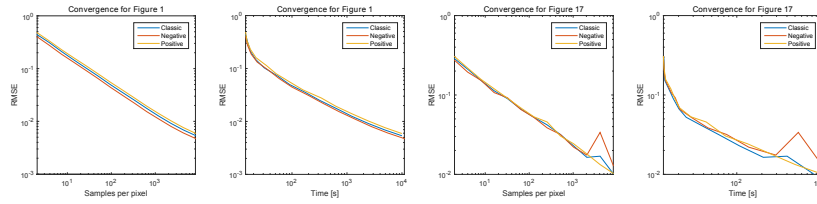


Fig. S.19. Convergence plots for the scenes in Figures 1 and 17, relating the RMSE with the number of samples and rendering time, respectively. Each scene is rendered with different types of media: a classic exponential medium, a negatively correlated medium, and a positively correlated medium modeled with our model in Section 5.2.

with respect to rendering time, since ray-geometry intersections dominate.

S.13 MONTE CARLO NUMERICAL SIMULATIONS

In order to gain understanding on the problem, illustrate the results, and compare our solutions against a ground truth, we computed a number of simulations on procedurally generated explicit media. This allowed us to investigate on the differences on the probability distribution of extinction $p(t)$ between scatterers and sources (Section 4), as well to study the effect of boundary conditions (Section 4.3). Here we explain the details of such simulations, including the definitions of the media, and include the full set of results of our simulations.

S.13.1 Modeling correlated scatterers

Since we are interested on the average behavior of $p(t)$, we procedurally generated different types of media in 2D. We opted for a two-dimensional problem since it is simpler but valid to our problem (extinction is a 1D problem), as has been shown in many previous works in transport related fields. Each media was formed by a number of circular scatterers with same (very small) radius r . For each realization of the 2D volume, we build a randomized procedural media. These procedural definitions were different for the case of positive and negative media.

- **Negatively Correlated Media:** Based on previous work on transport on Lorentz gases [Dumas et al. 1996]⁶, we generate a perfect negative media by deterministically defining the position of the particles in an array. We introduced the constraint of having each particle in the middle of an hexagon, where the closest neighbor particles where at the vertices of that hexagon. That ensured that the closest particles where all at the same distance. We then slightly displaced each vertex position to ensure that none of them masked any other particle along the propagation direction of the ray. Finally, we stochastically perturbed the position of the particles based on the desired degree of correlation η : We decided whether a particle should be perturbed with probability $p_p = 1 - |\eta|$, and perturbed its position \mathbf{x} as $\mathbf{x} = \mathbf{x}_0 + \omega s$, where \mathbf{x}_0 is the particle original position, ω is a unit vector uniformly sampled in the circle of directions, and $s = -\log(\xi)(1 - |\eta|)^2$ with ξ a uniform random number.

- **Positively Correlated Media:** Here we follow the approach of Shaw et al. [2002] and Larsen and Clark [2014]: We select the position of a first particle \mathbf{x}_0 by uniformly random sampling the unit square. Then, we begin a random walk from this initial position, so that the position \mathbf{x}_i of a particle $i > 0$ is computed as $\mathbf{x}_i = \mathbf{x}_{i-1} + \omega s$, where ω is a unit vector uniformly sampled in the circle of directions, and $s = -\log(\xi)(1 - \eta)^2$ with ξ a uniform random number and $\eta \in (0, 1)$ the degree of positive correlation.

In both cases, we use a periodic boundary condition following previous work [Shaw et al. 2002]. Note that we did not impose a minimum distance of particles (that could be another form of negative correlation by using a dart-throwing sampling approach; we did so to avoid introducing some form of correlation when each of the approaches converge to the uncorrelated behavior (i.e. $\eta \rightarrow 0$); however, given the small radii of the simulated particles (10^{-5} , distributed in a unit squared medium) we found that they were unlikely to intersect each other.

In the following, we show numerical solutions for source-to-scatterer and scatterer-to-scatterer probability distributions of extinction and transmittance (Section S.13.2), as well as simulations on the medium-to-medium boundary conditions (see Section 4.3) for a variety of different media correlations.

S.13.2 Source-to-Scatterer and Scatterer-to-Scatterer Extinction

Figures S.20 and S.21 show a series transmittances $T(t)$ for a source term at the boundary of the medium, and for scatterer-to-scatterer transport, respectively. Each of them has been computed for a different level of correlation $\eta_1 \in [-1, 0.9]$. We have simulated each of them by averaging 2000 iterations each iteration with a different randomly generated medium, and 1000 samples per iteration. The samples from the source $Q(\mathbf{x}, \omega_\theta)$ where traced from the boundary of the medium, for a given direction θ . In contrast, the samples for the scatterer-to-scatterer extinction were traced from the scatterers, by randomly selecting the scatterer of origin, and with a random direction.

S.13.3 Boundary Conditions

Figures S.22 and S.23 shows a wider range of results for the media-to-media boundary, complementing those in Figure 9, for $\eta_1 \in [-1, 0.9]$. We follow the same procedure as in Figure S.20, with a change of media at distance $t = 20$.

⁶A Lorentz gas is a periodic array of scatterers forming a lattice.

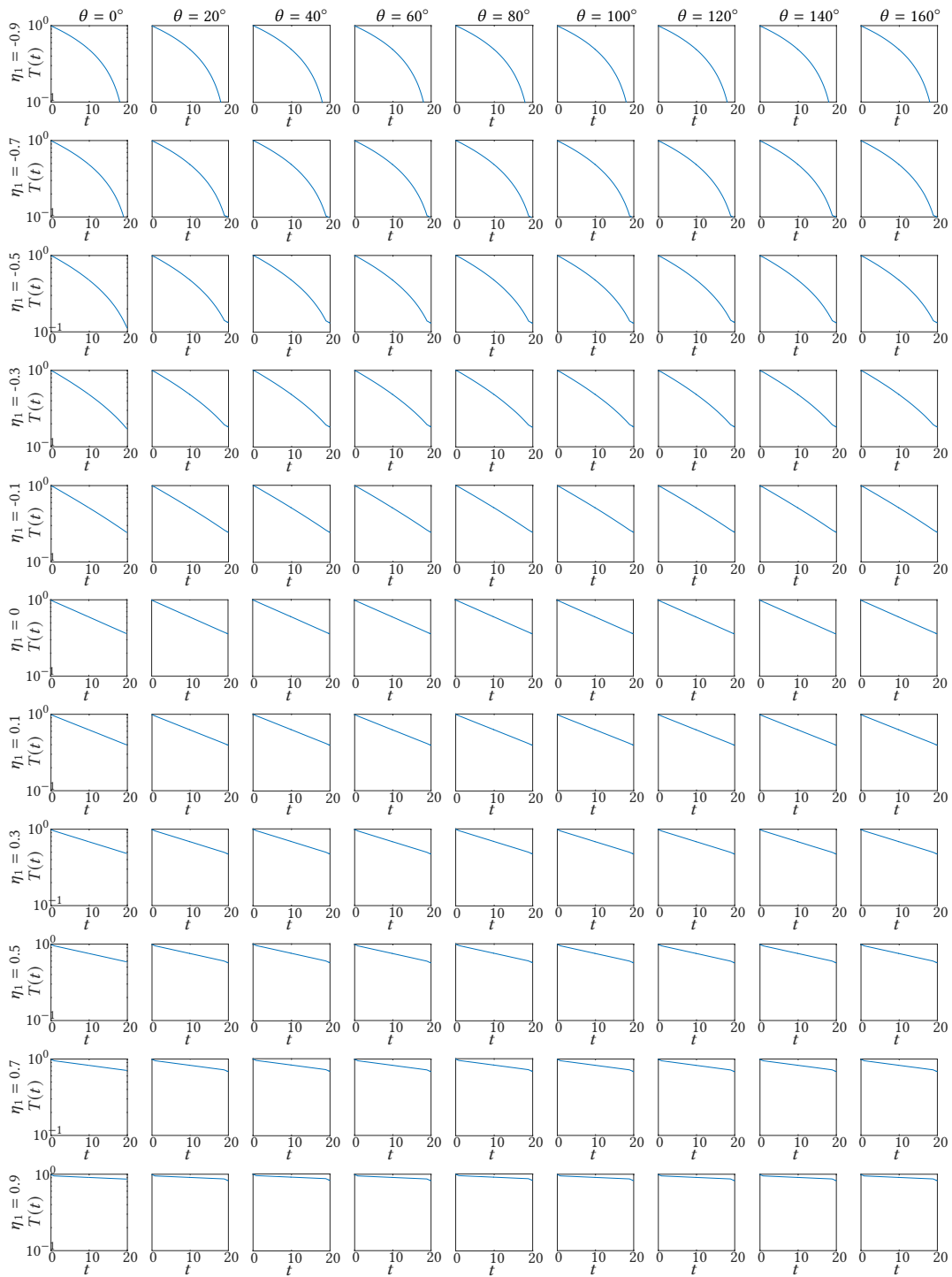


Fig. S.20. Monte Carlo simulations of the transmittance $T_Q(t)$ from rays with origin at sources, for infinite media with correlation varying from $\eta_1 \in [-1, 0.9]$, in logarithmic scale, for different angles θ .

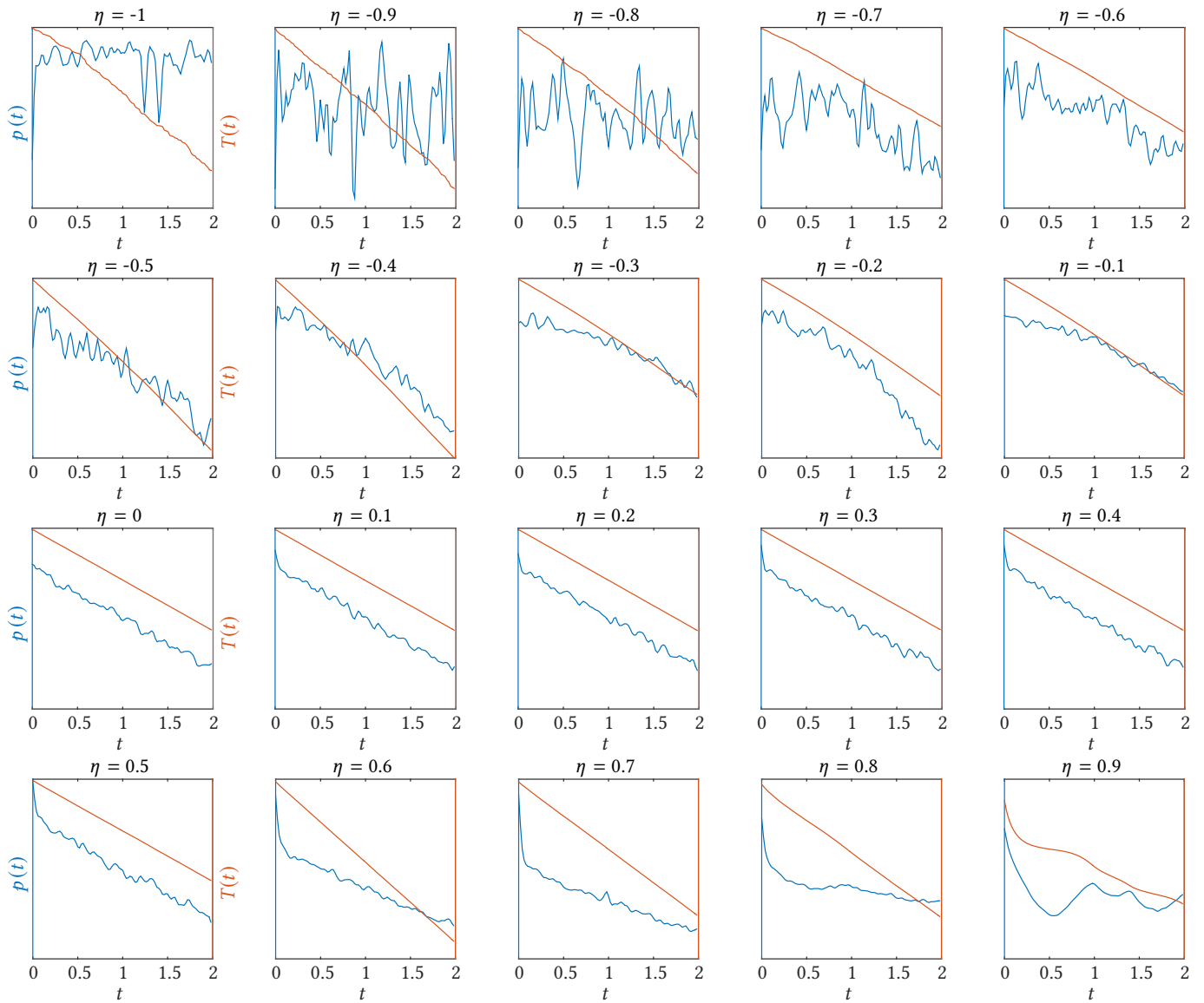


Fig. S.21. Monte Carlo simulations of the probability distribution of extinction $p_S(t)$ (blue) and transmittance $T_S(t)$ (orange) from rays with origin at scatterers, for infinite media with correlation varying from $\eta_1 \in [-1, 0.9]$, in logarithmic scale.

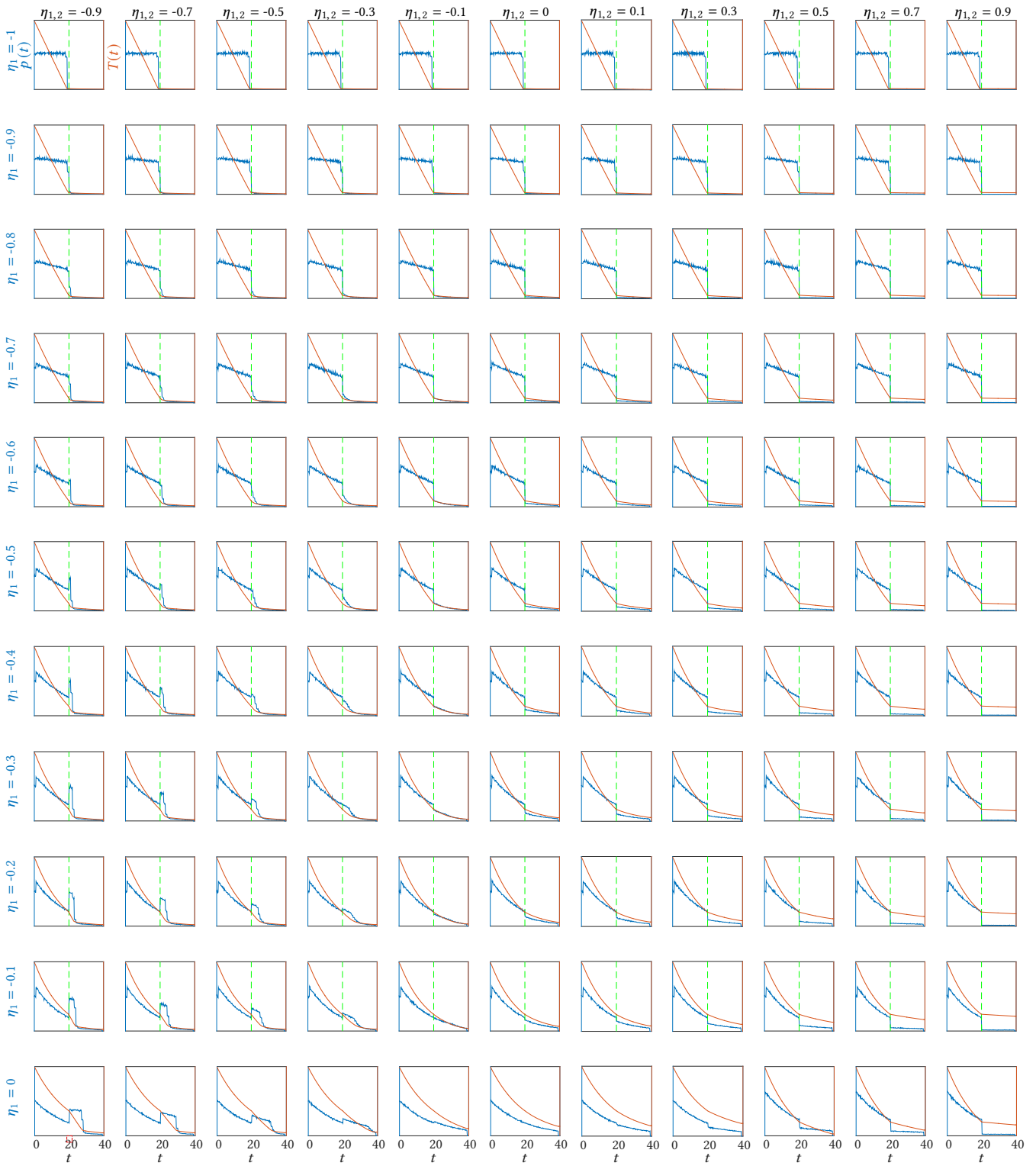


Fig. S.22. Monte Carlo simulations for the medium-to-medium boundary (marked as a green dashed line), showing the probability distribution of extinction $p(t)$ (blue), and transmittance $T_Q(t)$ (orange), for original media with correlation $\eta_1 \in [-0.9, 0]$, and second media defined so that the correlation between both media $\eta_{1,2} \in [-0.9, 0.9]$ infinite media with correlation varying from $\eta_1 \in [-1, 0.9]$.

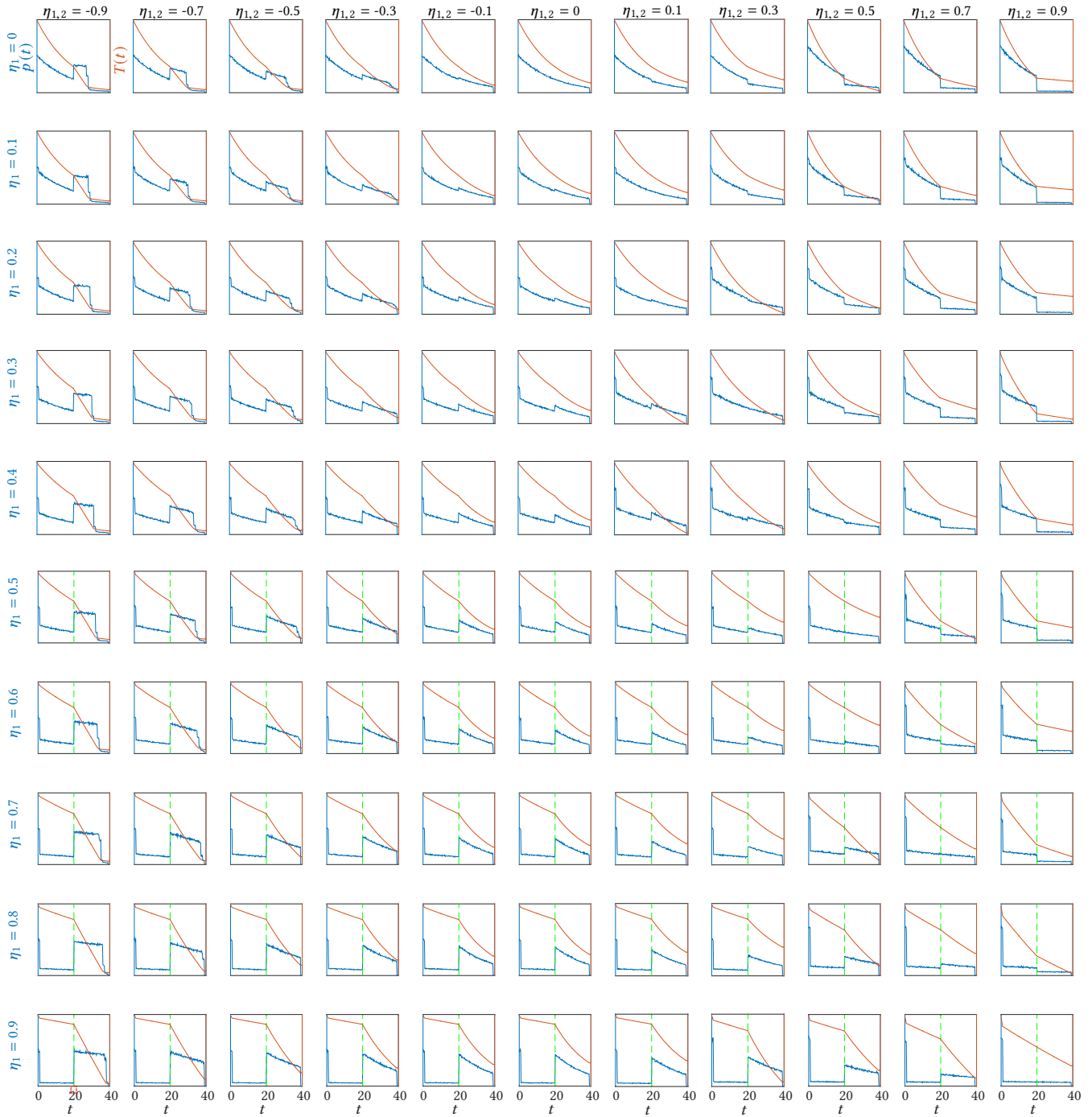


Fig. S.23. Monte Carlo simulations for the medium-to-medium boundary (marked as a green dashed line), showing the probability distribution of extinction $p(t)$ (blue), and transmittance $T_Q(t)$ (orange), for original media with correlation $\eta_1 \in [0, 0.9]$, and second media defined so that the correlation between both media $\eta_{1,2} \in [-0.9, 0.9]$ infinite media with correlation varying from $\eta_1 \in [-1, 0.9]$.

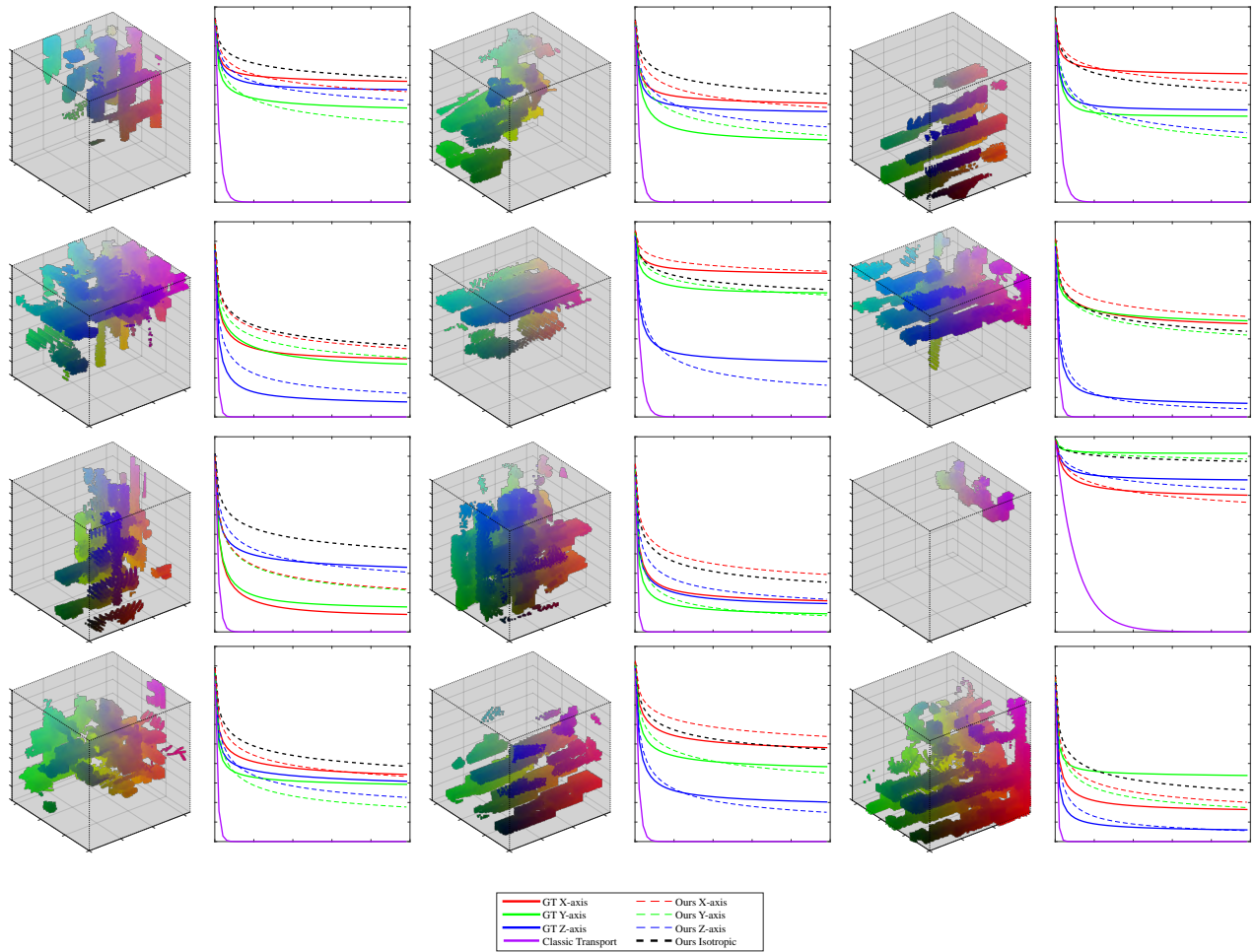


Fig. S.24. Additional examples of transmittance in high-resolution volumes of locally-correlated media (procedurally generated after [Lopez-Moreno et al. 2015]). Beams of light travel through each volume, aligned in succession to the x , y , and z axes. Ground truth transmittance (red, green, and blue solid lines) has been computed by brute force regular tracking [Amanatides and Woo 1987], while our simulation (dotted lines) uses the gamma distribution proposed in Equation 19. Classic transport governed by the RTE significantly overestimates extinction through the volume, resulting in an exponential decay (purple line). In contrast, our model matches ground-truth transmission much more closely. The black dotted line is the result of isotropic correlation, which is clearly also non-exponential.